Materials Science & Engineering B - Advanced Functional Solid-State Materials
Impact factor = 4.051

https://www.journals.elsevier.com/materials-science-and-engineering-b

Accepted February 18th 2022

INFLUENCE OF MAGNETIZATION, VARIABLE VISCOSITY AND THERMAL CONDUCTIVITY ON VON KARMAN SWIRLING FLOW OF H_2O-FE_3O_4 AND H_2O-Mn-$ZNFe_2O_4$ FERROMAGNETIC NANOFLUIDS FROM A SPINNING DISK: *SMART SPIN COATING SIMULATION*

S.O. Salawu[1]

[1]*Department of Physical Science, College of Pure and Applied Sciences, Landmark University, Omu-aran,* ***Nigeria****.*
Email: kunlesalawu2@gmail.com

MD. Shamshuddin[2*]
[2]*Department of Mathematics, Vaagdevi College of Engineering (Autonomous), Warangal-506005, Telangana,* ***India.***
Email: shammaths@gmail.com, shamshuddin_md@vaagdevi.edu.in

O. Anwar Bég[3]
[3]*Multi-physical Engineering Sciences Group (MPESG), Mechanical Engineering Department, Salford University, Manchester, M54WT,* ***UK****.*
Email:O.A.Beg@salford.ac.uk

**Corresponding author: email- shamshuddin_md@vaagdevi.edu.in*

Abstract: Motivated by smart (functional) nano-ferromagnetic spin coating applications**,** a theoretical study is described for steady swirling Von Karman thermo-magnetic water-based flowing nanoliquids containing ferromagnetic nanoparticles from a rotating disk in Darcian permeable media. The Odenbach formulation is deployed for magnetic field-dependent viscosity and the Hooman-Gurgenci model is used for variable thermal conductivity. The governing mass, momentum and temperature equations are converted into nonlinear-coupled ordinary derivative momentum and energy equations via appropriate similarity transformations with appropriate boundary conditions. A nanoscale Tiwari-Das formulation is deployed for the fractional volume nanoparticle effects. The resulting boundary value ordinary differential problem is solved by a Galerkin weighted residual method (GWRM) along with Simpson's one-third rule. Verification of the GWRM solutions is achieved with numerical shooting quadrature (MAPLE) and very good correlation is demonstrated. Ferromagnetic Fe_3O_4 nanofluid is observed to achieve superior thermal conductivity enhancement relative to ferromagnetic Mn-$ZnFe_2O_4$ nanofluid. Increasing permeability parameter (K) enhances axial, radial and tangential velocity magnitudes and, in all cases, the Fe_3O_4 -water ferromagnetic nanofluid achieves greater values than the Mn-$ZnFe_2O_4$ -water ferromagnetic nanofluid, in particular at intermediate distances from the disk surface (axial coordinate). Increasing magnetic field intensity (δ) substantially modifies the viscosity and produces a consistent retardation in both axial and radial velocity whereas it weakly enhances the tangential velocity field. With greater ferromagnetic interaction number (β) axial velocity is enhanced strongly, and radial velocity is also boosted. However tangential velocity is slightly reduced, and temperature is strongly suppressed for both ferromagnetic nanofluids.

Keywords: *Von Karman swirling disk flow; Ferrofluids; ferromagnetic nanoparticles; Viscosity and thermal conductivity variation; Galerkin weighted residual method (GWRM); Darcy porous medium; smart functional coating systems.*

1. Introduction

A ferrofluid [1] is a colloidal suspension of stable ferromagnetic nanometric sized or ferromagnetic oxide particles, in a working base fluid such as oil, water etc. The ferromagnetism characteristic is changed to super-para-magnetism by particle size decreasing to a nanometer size. Ferrofluids are therefore *smart liquids materials* which can be manipulated via the imposition of an external magnetic field, and this therefore allows careful manipulation of the thermophysical characteristics for a range of emerging applications including smart coatings, hybrid rocket fuels, intelligent lubrication for dampers (seismic, helicopters etc.) and robotics.

In ferrofluids, magnetic field strongly influences viscosity [2]. The viscosity of such fluids produces *rheological* behavior, which exerts a key role in modifying thermofluid characteristics. These strongly magnetized (ferrofluids) are finding increasing applications in modern systems, as they possess *functional* properties. In for example, biomedical applications, they appear in hyperthermia, magnetic separation, MRI and other technologies. With some conditions, Fe_3O_4 and $\gamma - Fe_3O_4$ suspensions colloidal have been deeply studied because they were taken to be biocompatible. A key emerging area of interest is smart functional ferromagnetic nano-coatings. These feature many different techniques for achieving a homogenous and durable coating on critical engineering components including spin coating [3] in which rotating components e. g. disks, cones, spheres etc., are finished with a ferromagnetic nanomaterial surface layer. Many excellent studies of ferrofluid coating flows have been communicated including Zahn [4], Torres-Díaz and Rinaldi [5], Tian et al. [6] and Kuroki [7] for biomedical implants. Extensive details of the preparation of ferromagnetic nanofluid coatings are given in Kole and Khandekar [8] and Arana et al. [9].

The science of *ferro-hydrodynamics* is used to simulate ferromagnetic liquids and has been lucidly established in the monograph by Rosensweig [10]. A number of researches have also been carried out to characterize the behaviour rheology of ferrofluids [11], in which the influence of variable conductivity, rotational viscosity and magnetization force have been addressed. Depending on different target usefulness, preparation of ferrofluids in solvents can be done in many ways, which includes glycerol, aromatics, paraffin, water and others. The nanoparticles diameter mean in ferrofluids differs from 3 to 15 nanometer sizes as elaborated in [2]. The nanoparticle numbers in a suspension colloidal is of 10^{23} /m^3 order. Theoretical and experimental investigations of magnetic fluid viscosity have been considered by various scientists including [11, 12]. In their study [13, 14] established that the ferromagnetic density

of nanoparticles in the transferring fluid also distresses magnetic fluid viscosity. A number of interesting articles have also examined transport phenomena in based water ferro-liquids under the magnetic fields action [15-19].

As noted earlier, spin coating [3] is an important industrial procedure for deploying ferromagnetic nano-coatings efficiently. In the case of thin film deposition on rotating disks, the regime generated is known as Von Karman swirling flow [20]. In such flows, a boundary layer regime is produced which acts like a pump in which fluid is drawn axially and exits radially along the disk surface. Many diverse investigations of multi-physical swirling disk flows have been communicated. Mishra et al. [21] used a non-Fourier Cattaneo-Christov heat flux formulation and perturbation technique to analyze the momentum and thermal characteristics in dual disk swirling flow. Anwar Bég et al. [22] adopted PSPICE thermal-electro software to analyze the slip and wall transpiration effects in radiative magnetized Von Karman swirling flows. Hayat et al. [23] analyzed the viscous swirling flow and thermal diffusion in two stretchable rotating disks observing that increasing Prandtl number and non-Fourier heat relaxation term suppresses temperatures. More recently *nanofluid swirling flows* have also received some attention. Turkyilmazoglu [24] used the Tiwari-Das nanoscale model and a collocation Chebyshev spectral computational integration method to compute the Von Karman swirling flow of TiO_2, Al_2O_3, CuO, Ag and Cu, and water-based nanofluids, observing that a good thermal conductivity augmentation is achieved with Cu nanoparticles. Anwar Bég et al. [25] studied tangential and radial slip effects on bio-nanocoating swirl flows with the Buongiorno nanoscale two-component model and wall mass flux and gyrotactic microorganism effects. Very recently, Umavathi et al. [26] employed bvp4c MATLAB quadrature Lobatto to solve the time-dependent magnetohydrodynamic nano-lubricant flow in a disk with mixed boundary conditions. These studies however did not consider *ferrofluid* swirling flows. Several excellent investigations of ferrofluid dynamics from rotating disks have however been communicated. Ram and Kumar [27] used MATLAB shooting techniques to simulate the axisymmetric ferrofluid flow due to rotating disk in a porous medium. They evaluated the effect of magnetic viscosity parameter and porosity on radial and azimuthal skin friction and also boundary layer displacement thickness. Bhandari [28] used the COMSOL Multiphysics platform to compute the rotating disk flowing ferrohydrodynamic and a rod with applications in liquid seal coatings, observing that magnetization force and the rod radius plays a vital part in the fluid flowing rate field and thermal diffusion augmentation. Mustafa et al. [29] adopted finite implicit difference method to compute the performance of Mn-Zn ferrite ferroparticles, cobalt ferrite and magnetite in boundary layer three-dimensional stagnation

point flowing ferrofluid from a circular rotating stretchable disk under external magnetic field. They found that radial flow deceleration is generated for magnetite ferroparticle (Fe_3O_4) whereas tangential flow acceleration and temperature elevation is produced with increasing volume fraction parameter. They also showed that radial wall coefficient friction and local wall temperature gradient of magnetize ferroparticle (Fe_3O_4) due to higher density and thermal conductivity properties. Further numerical investigations of ferromagnetic nanofluid Von Karman swirling flows include Ellahi et al. [30] (who also studied oscillation and stretching effects of the rotating disk), Mustafa et al. [31] (who considered radiative heat flux effect) and Loganayagi and Kameswaran [32] (who reflected on the Hall current, slip impact and Hematite (Fe_2O_3) and iron/Cobalt hybrid nanoparticles with Motor Oil 10W30 base fluid). Several numerical approaches have been used to compute nanofluid heat transfer properties under heat variable conductivity and magnetic field effects. Interesting studies include Ahmed et al. [33] (spinning coaxially disks), Hazarika and Borah [34] (stretchable radial disk), Konch and Hazarika [35] (double-phase rotating disk of ferromagnetic flowing fluid), Shaw et al. [36] (entropy analysis on rotating disk), Das et al. [37] (entropy analysis in radially stretching disk), and Shateyi and Makinde [38] (stagnation flow on radially stretching heated disk).

The studies reported earlier, have neglected however the comparative performance of Fe_3O_4 -water ferromagnetic and Mn-$ZnFe_2O_4$ -water ferromagnetic nanofluids in porous media, and also variable viscosity and thermal conductivity effects in Von Karman swirling coating flow. This is the novelty of the present study. The characteristics of nanoparticles and water (specific heat, heat conduction and density) are investigated for current variable formulation. The heat conduction of the nanoliquid differs with temperature whereas the viscosity is dependent on applied magnetic field. A nanoscale Tiwari-Das formulation is deployed for fractional volume nanoparticle impacts. The solutions to the converted ordinary derivative boundary value equations are obtained numerically with a Galerkin weighted residual method (GWRM) along with Simpson's one-third rule. Computed outcomes for the flow rate and heat dispersions are portrayed in graphical term presentation and tables. Verification of the GWRM solutions is achieved with benchmarking via existing studies and very good correlation is demonstrated. The flow dimensions of the velocity distributions and heat transfer are analyzed. The present simulations find immediate applications in spin coating of engineering components with smart ferromagnetic nanofluids [39-41] and on variable viscosity nanofluids [42]. The present study therefore extends the existing literature via the inclusion of variable heat conduction and viscosity effects, which are shown to have a significant influence on coating thermofluid transport characteristics.

2. Ferromagnetic nanofluid Von Karman swirling coating flow model

The water-based ferromagnetic nanofluid swirling flow from a rotating disk in the existence of magnetic field in a porous medium is considered for magnetic nanoparticles (Fe_3O_4, Mn-$ZnFe_2O_3$). For rotational flow, a cylindrical coordinate (r,ϕ,z) is adopted for the formulation of mathematical model, which is visualized in **Figure 1**. The disk plane is situated at $z=0$ and the disk spins with unvarying angular velocity, Ω about the vertical axis, z. Applied magnetic field acts in both the tangential and radial directions, as characteristic of ferrofluid dynamics [1]. The permeable media is taken to be homogenous and isotropic, and Darcy's law is adopted. Temperature-dependent heat source/sink effects are also included. From the aforementioned assumptions, the continuity model, equations of radial, tangential momentum and heat flow equation in an axisymmetric boundary layer flow of ferromagnetic nanofluid from a rotating disk are obtained by extending and amalgamating earlier models of Bandari [28] and Abdel-Wahed et al. [43], to include variable heat conduction and viscosity to yield:

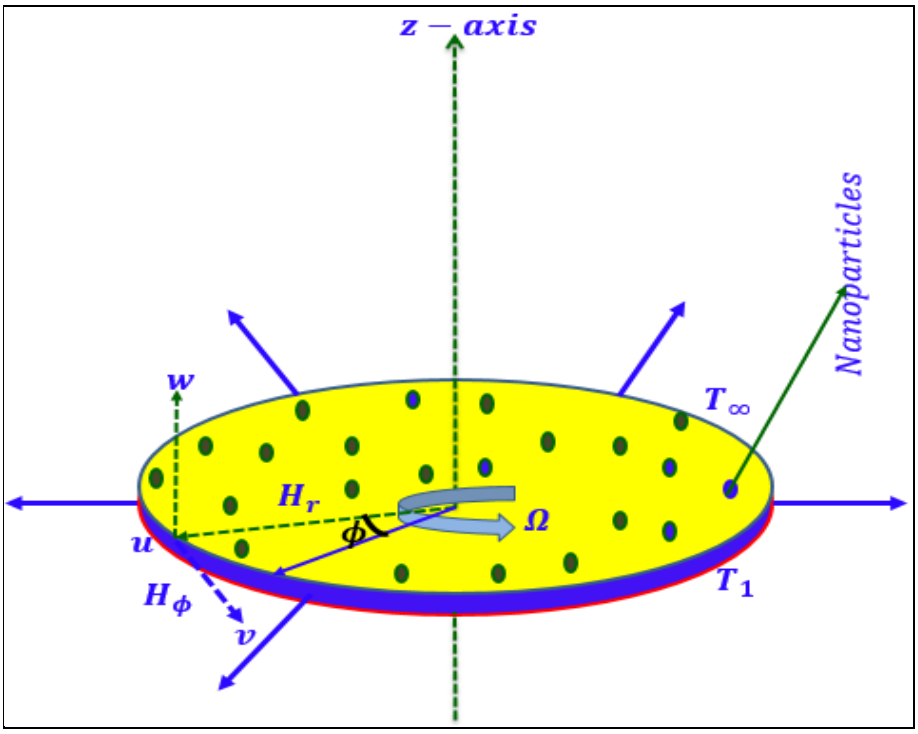

Figure 1: Physical model for swirling flow of ferromagnetic nanoliquid from a spinning disk in porous media

$$u_r + w_z + \frac{u}{r} = 0, \tag{1}$$

$$\rho_{nf}\left(u\,u_r + w\,u_z - \frac{v^2}{r}\right) = -p_r - \mu_0 M\,H_r + \mu_{nf}\left\{1+\frac{3}{2}\phi_1\frac{\delta-\tanh\delta}{\delta+\tanh\delta}\right\}\left(u_{zz}+\frac{1}{r}u_r+u_{rr}-\frac{u}{r^2}\right) - \frac{\mu_{nf}}{k_0}\left\{1+\frac{3}{2}\phi_1\frac{\delta-\tanh\delta}{\delta+\tanh\delta}\right\}u, \tag{2}$$

$$\rho_{nf}\left(u\,v_r + w\,v_z + \frac{uv}{r}\right) = -\mu_0\,\frac{M}{r}H_\phi + \mu_{nf}\left\{1+\frac{3}{2}\phi_1\frac{\delta-\tanh\delta}{\delta+\tanh\delta}\right\}\left(v_{zz}+\frac{1}{r}v_r+v_{rr}-\frac{v}{r^2}\right) - \frac{\mu_{nf}}{k_0}\left\{1+\frac{3}{2}\phi_1\frac{\delta-\tanh\delta}{\delta+\tanh\delta}\right\}v, \tag{3}$$

$$(\rho c_p)_{nf}\left(u\,T_r + w\,T_z\right) = -\mu_0 T\,M_T\left(u\,H_r + \frac{1}{r}v\,H_\phi\right) + \frac{k(T)}{r}T_r + \left(k(T)\,T_r\right)_r + \left(k(T)\,T_z\right)_z + Q_T^*\left(T-T_c\right) \tag{4}$$

The prescribed disk surface boundary conditions (coating plane) for the far free flow are:

$$\left.\begin{array}{llllll} at & z=0; & u=0, & v=\Omega r, & w=0, & T=T_w \\ at & z\to\infty; & u\to 0, & v\to 0, & T\to T_\infty, & P=P_\infty \end{array}\right\} \tag{5}$$

Here μ denotes dynamic viscosity, δ represents magnetic field intensity, k_0 connotes porosity constant of the porous medium (hydraulic conductivity), μ_0 is the free space porosity, M is the magnetization term, H stands for intensity of magnetic field, c_p represents specific heat, ρc_p denotes heat capacity, T stands for temperature, k is heat conductivity, $k(T)$ denote heat dependent conductivity, Q_T^* signifies coefficient of temperature-reliant heat sink/source, (Ω) stands for disk angular velocity and (T_w) represents disk temperature.

The nanofluid viscosity is a function of magnetic field and following Oldenbach [44] is written as:

$$\mu_{nf}\left(H\neq 0\right) = \mu_f\left\{1+\frac{5}{2}\phi_1\right\}\left(1+\frac{3}{2}\phi_1\frac{\delta-\tanh\delta}{\delta+\tanh\delta}\right) \tag{6}$$

In the present formulation, the terms $\mu_{nf}\left(1+\frac{3}{2}\phi_1\frac{\delta-\tanh\delta}{\delta+\tanh\delta}\right)$ signifies the magnetic field - dependent viscosity. Without magnetic field, the expression $1+\frac{3}{2}\phi_1\frac{\delta-\tanh\delta}{\delta+\tanh\delta}$ vanishes and nanoparticles rotates with angular velocity.

The nanofluid variable heat conduction depends on temperature and this is simulated following Hooman and Gurgenci [45] as:

$$k(T) = k_{nf}\left\{1+\varepsilon\frac{T-T_\infty}{T_w-T_\infty}\right\} \tag{7}$$

In which ε represents heat variable conductivity term.

The magnetic field radial and tangential modules are defined as expresses:

$$\begin{aligned} H_r &= -\frac{\partial\psi}{\partial r} = \frac{\delta_0}{2\pi}\frac{\cos\phi}{r^2}, \\ H_\phi &= -\frac{\partial\psi}{\partial\phi} = \frac{\delta_0}{2\pi}\frac{\sin\phi}{r}, \end{aligned} \tag{8}$$

Here δ_0 connotes magnetic field strength, (r,ϕ) designate radial and tangential coordinates.

The total magnetic field intensity [28] is computed as:

$$H = \sqrt{(H_r)^2 + (H_\phi / r)^2} = \frac{\delta_0}{2\pi\, r^2} \tag{9}$$

The rates of change of tangential and radial modules of the intensity of magnetic field are given as:

$$\begin{aligned} H_r &= -\frac{\delta_0}{\pi\, r^3}, \\ H_\phi &= 0 \end{aligned} \tag{10}$$

Considering magnetization, which is assumed to behave as a temperature *linear* function following Rosensweig [10] as:

$$M = K_1(T_c - T) \tag{11}$$

Here K_1 represents the pyro-magnetic coefficient and T_c is Curie temperature.

The density effectiveness (ρ_{nf}), viscosity (μ_{nf}), heat diffusivity (α_{nf}) and heat nanofluid capacity [28] can be expressed as follows where ϕ_1 is nanoparticle volume fraction:

$$\begin{aligned} &\rho_{nf} = (1-\phi_1)\rho_f + \phi_1\,\rho_s, \quad \mu_{nf} = \frac{\mu_f}{(1-\phi_1)^{5/2}}, \quad \alpha_{nf} = \frac{k_{nf}}{(\rho c_p)_{nf}}, \\ &(\rho c_p)_{nf} = (1-\phi_1)(\rho c_p)_f + \phi_1 (\rho c_p)_s, \frac{k_{nf}}{k_f} = \frac{k_s + 2k_f - 2\phi_1(k_f - k_s)}{k_s + 2k_f + \phi_1(k_f - k_s)} \end{aligned} \tag{12}$$

The fluid properties for the considered base fluid (water) and ferromagnetic nanoparticle to be deployed in the spin coating simulations are depicted in **Table 1**.

Table 1: Thermophysical property of base fluid and nanoparticles.

	ρ (kg/m^3)	c_p (J/Kg-K)	k(W/m-K)
Water	997.1	4179	0.613
Fe_3O_4	5200	670	6
Mn-ZnFe_2O_4	4700	1050	3.9

To render the conservation equations dimensionless and self-similar, the following Von Karman transformations are invoked [43]:

$$\left.\begin{aligned} &u = r\,\Omega\, f'(\eta), \quad v = r\,\Omega\, g(\eta), \quad w = -\sqrt{2\,\Omega\, \nu_f}\, f(\eta), \\ &p = P_\infty + 2\,\Omega\,\mu_f\, P(\eta),\ T = T_c + (T_w - T_c)\,\theta(\eta),\ \eta = z\sqrt{\frac{2\,\Omega}{\nu_f}} \end{aligned}\right\} \tag{13}$$

Where $f(\eta)$, $f'(\eta)$, $g(\eta)$, $P(\eta)$, λ, θ and η stands for dimensionless axial, radial and tangential velocities, non-dimensional pressure, non-specific pressure gradient, dimensionless temperature and axial coordinate.

Applying the aforementioned definitions, the transformed momentum and temperature equations with the resultant boundary conditions emerge as:

$$\frac{K_1}{K_2\ K_3}\left(2f''' - \frac{1}{K}f'\right) + \left(2f\ f'' - (f')^2 + g^2\right) + \beta\theta = 0 \tag{14}$$

$$\frac{K_1}{K_2\ K_3}\left(2g'' - \frac{1}{K}g\right) + 2f\ g' - 2\ f'\ g = 0 \tag{15}$$

$$K_4\left[(1+\varepsilon\,\theta)\,\theta'' + \varepsilon\,(\theta')^2\right] + K_5\,\mathrm{Pr}\ f\ \theta' - \mathrm{Pr}\ \beta_1\ f' - \mathrm{Pr}\,\beta_2\ f'\,\theta + \mathrm{Pr}\ S_T\ \theta = 0 \tag{16}$$

The transformed boundary conditions assume the form:

$$\begin{aligned} &f(0) = 0, \quad f'(0) = 0, \quad g(0) = 1, \quad \theta(0) = 1, \\ &f'(\infty) = 0, \quad g(\infty) = 0, \quad \theta(\infty) = 0 \end{aligned} \tag{17}$$

Here the primes denote differentiation w.r.t η and the following definitions apply:

$$\begin{aligned} &K_1 = \left\{1 + \frac{3}{2}\phi_1\frac{\delta - \tanh\delta}{\delta + \tanh\delta}\right\},\ K_2 = (1-\phi_1)^{2.5},\quad K_3 = \left\{1 - \phi_1 + \phi_1\frac{\rho_s}{\rho_f}\right\}, \\ &K_4 = \left\{\frac{k_s + 2k_f - 2\phi_1\,(k_f - k_s)}{k_s + 2k_f + 2\phi_1\,(k_f - k_s)}\right\},\quad K_5 = \left\{1 - \phi_1 + \phi_1\frac{(\rho c_p)_s}{(\rho c_p)_f}\right\} \end{aligned} \tag{18}$$

The dimensionless variables taking in Eqns. (14) - (17) are as describes:

$$K=\frac{k_0\ \Omega}{\nu_f},\ \mathrm{Pr}=\frac{(\rho c_p)_f\ \nu_f}{k_f},\beta=\frac{\mu_0\ K_a\ \delta_0(T_1-T_2)}{\pi\ \rho_f\ \Omega^2\ r^4},\ \beta_1=\frac{\mu_0\ K_a\ \delta_0\ T_c}{2\ \pi\ r^2(\rho c_p)_f(T_w-T_c)},$$
$$\beta_2=\frac{\mu_0\ K_a\ \delta_0}{2\ \pi\ r^2(\rho c_p)_f},S_T=\frac{Q_T^*}{2\,(\rho c_p)_f\ \Omega} \tag{19}$$

Here K denotes permeability parameter (porous medium characteristic), Pr denotes Prandtl number, (β,β_1,β_2) denote the ferromagnetic interaction numbers, and S_T denotes the temperature-dependent heat source/sink parameter.

In coating designs, important wall behavior can be computed using tangential and radial wall friction and thermal gradient rate. These quantities are expressed respectively, as follows:

$$\tau_s=\mu_{nf}\left\{u_z\right\}_{z=0},\tau_w=\mu_{nf}\left\{v_z\right\}_{z=0},q_w=-\left(K(T)\,T_z\right)_{z=0} \tag{20}$$

The corresponding expressions for *non-dimensional radial, tangential stresses and thermal gradient* for the flowing fluid are as stated:

$$C_f=\frac{\mu_{nf}}{\rho_f(r\,\Omega)^2}(u_z)_{z=0}\Rightarrow\sqrt{\mathrm{Re}}\,C_f=\frac{1}{K_2}\,f''(0),$$
$$C_g=\frac{\mu_{nf}}{\rho_f(r\,\Omega)^2}(v_z)_{z=0}\Rightarrow\sqrt{\mathrm{Re}}\,C_g=\frac{1}{K_2}\,g'(0), \tag{21}$$
$$Nu=\frac{q_w}{k_f(T_w-T_c)}\Rightarrow\frac{Nu}{\sqrt{\mathrm{Re}}}=K_4\ \ \theta'(0),$$

It is essential to cognizes of thermal coating operations, the Nusselt number which measures thermal transport gradient at the surface of the disk can also be employed to quantify the relative to thermal convection to heat conduction.

3. GWRM Numerical solution methodology and validation

The procedure of weighted residuals along with a Galerkin scheme i.e., Galerkin weighted residuals method (GWRM) is used to derive numerical solutions for the emerging highly nonlinear dimensionless equations with associated boundary conditions (14) to (17) and the engineering quantities. This approach has been employed recently in a number of other studies, which includes Oderinu and Aregbesola [46], Salawu et al. [47] (on branch-chain thermal reactive viscoelastic flows) and Salawu and Okoya [48] (on thermal reactive-diffusion in a cylinder). To determine the sensitivity of the entrenched terms, a polynomial basis function is defined for the $f(\eta),g(\eta)$ and $\theta(\eta)$. That is:

$$f(\eta)=\sum_{i=0}^{j} a_i\,\eta^i,\;\; g(\eta)=\sum_{i=0}^{j} b_i\,\eta^i,\;\; \theta(\eta)=\sum_{i=0}^{j} c_i\,\eta^i \tag{22}$$

Here j is a secure whole number and a_i, b_i and c_i are constants to be obtained.

In the weighted residual scheme, the base function is expected to satisfy the boundary conditions. Therefore, the boundary conditions i.e. Eqn. (17) are formulated on the base function of Eqn. (19) to give a system of seven linear equations in terms of a_i, b_i and c_i as follows:

$$a_0 = 0, \tag{23}$$

$$a_1 = 0, \tag{24}$$

$$a_1 + 10\,a_2 + 75\,a_3 + 500\,a_4 + 3125\,a_5 + 18750\,a_6 + 109375\,a_7 + 625000\,a_8 + 3515625\,a_9 + 19531250\,a_{10} = 0, \tag{25}$$

$$b_0 - 1 = 0, \tag{26}$$

$$b_0 + 5\,b_1 + 25\,b_2 + 125\,b_3 + 625\,b_4 + 3125\,b_5 + 15625\,b_6 + 78125\,b_7 + +390625\,b_8 + 1953125\,b_9 + 9765625\,b_{10} = 0, \tag{27}$$

$$c_0 - 1 = 0, \tag{28}$$

$$c_0 + 5\,c_1 + 25\,c_2 + 125\,c_3 + 625\,c_4 + 3125\,c_5 + 15625\,c_6 + 78125\,c_7 + +390625\,c_8 + 1953125\,c_9 + 9765625\,c_{10} = 0. \tag{29}$$

In addition, the base function is applied on the dimensionless equations to generate the residual equations. These equations are reduced as possible near to zero using the Galerkin integrating scheme in a range depending on the considered boundary conditions, according to Salawu et al. [47]. The $f(\eta), g(\eta)$ and $\theta(\eta)$ residuals are integrated over the domain using Simpson's one-third rule which circumvents the difficulty of direct integration to obtain a nonlinear system of equations in a_i, b_i and c_i. The obtained system of equations together with the enacted base functions for the boundary conditions are concurrently solved to determine the unknown a_i, b_i and c_i, which are then substituted in the polynomial basis function to have the required solution. Maple software is used to determine the unknown constants a_i, b_i and c_i, and provide complete numerical solutions to the problem. The exactness of the GWRM in solving the quasi-linear equations is established in **Table 2**. The GWRM solutions agree closely with the shooting method (Maple bvp4c quadrature) confirming confidence in the GWRM code.

Table 2: Results comparison of GWRM with numerical shooting method (MAPLE)

β_1	β_2	GWRM Results		Numerical shooting Results	
		$f''(0)$	$\theta'(0)$	$f''(0)$	$\theta'(0)$
0.5	1.0	1.640227	25.994457	1.640212	25.994449
2.0	1.5	1.085158	13.180761	1.085137	13.180745
3.0	2.0	0.844336	9.883323	0.844322	9.883312

Table 2 shows that radial skin friction function, $f''(0)$ is reduced with increasing ferromagnetic parameters β_1 and β_2 .However, there is a much greater decrease in Nusselt number function i. e., temperature gradient at the disk surface $\theta'(0)$ with increment in both ferromagnetic parameters. Stronger ferromagnetic effect (associated with the magnetization forces) therefore decelerates radial flow and heats the ferrofluid resulting in less transfer of thermal energy to the disk surface.

4. GWRM Results and discussion

The solution method for the non-dimensional boundary value problem of this study is done via the Galerkin weighted residual method (GWRM) along with Simpson's one-third method. The flow characteristics sensitivity of parameters variation are carried out with the following base (default) values $\phi_1 = 0.1, \delta = 0.2, K = 0.3, \beta = \beta_1 = \beta_2 = 1, K_1 = 1.0524,$ $\mathrm{Pr} = 3, \varepsilon = 0.1$ and $S_T = 1.0$. These values hold for all the computations unless otherwise stated on the graphs and are obtained from the quantitative theoretical investigation carried out associated studies by researchers [28, 43]. **Tables 3 and 4** portray the radial and tangential wall coefficient friction and thermal gradient results for various parameters, respectively, for Fe_3O_4 and Mn-$ZnFe_2O_4$- ferromagnetic water-based nanofluids.

Table 3: Skin friction and Nusselt number results for Fe_3O_4-nanoliquid for different parameters

β	K	δ	ϕ_1	c_f	c_g	Nu
1.5	0.3	0.2	0.1	1.4110470876	-1.4237937881	30.7712960414
2.0				1.5164709650	-1.4298287757	22.7432208157
	0.5			1.5031749301	-1.1891898361	18.2165833451
	0.7			1.4928763982	-1.0715776432	16.3179868420
		0.4		1.5150489780	-1.4293937140	22.8074578697
		0.6		1.5128523882	-1.4287231916	22.9071862957
			0.03	1.6194456289	-1.4633686616	18.6941881579
			0.07	1.5605813960	-1.4437086938	20.8703450518

Table 3 depicts that radial wall friction, c_f is raised with rising values of ferromagnetic parameter β (which is the reverse trend to that induced with increment in ferromagnetic parameters β_1 and β_2 in Table 1) whereas the tangential skin friction, c_g is reduced (tangential flow deceleration). Nusselt number is also strongly decreased with greater values of ferromagnetic parameter, β in consistency with the results for the other ferromagnetic parameters β_1 and β_2 computed in Table 1. Increasing permeability parameter, *K*, produces a strong radial flow acceleration i. e. greater c_f whereas it induces a decrease in tangential skin friction, c_g and also suppresses Nusselt number values. With elevation in the magnetic field intensity parameter, δ , there is a weak increase in radial skin friction, c_f whereas there is a reduction in tangential skin friction, c_g and also a sharp decline in Nusselt number. With a decrease in Fe_3O_4 nanoparticle volume fraction, ϕ_1 there is a boost in radial skin friction, c_f and a decrement in tangential skin friction and Nusselt number. Smaller volume fractions therefore reduce the heat transfer to the disk surface whereas larger volume fractions increase it.

Table 4 shows that for Mn-$ZnFe_2O_4$ ferromagnetic nanofluid, radial skin friction, c_f is weakly reduced with increasing Prandtl number whereas tangential skin friction c_g is slightly increased; there is a very strong reduction however in Nusselt number. With greater thermal conductivity parameter (ε) there is a significant reduction in radial skin friction, c_f and Nusselt number, but a weak increase in tangential skin friction, c_g . Decreasing values of temperature-dependent heat source parameter (S_T) produce a decrement in radial skin friction, c_f , a weak increase in tangential skin friction, c_g (less negative values are computed) and a significant plummet in Nusselt number magnitudes. $S_T > 0$ implies heat source is present and this boosts temperatures which thickens the thermal boundary layer and reduces heat transfer to the disk surface (wall) i. e. lower Nusselt numbers (the case of heat sink i.e. $S_T < 0$ is not analyzed here). Finally, with increasing ferromagnetic parameter β_1 the radial skin friction, c_f is suppressed, there is an increase in tangential skin friction, c_g (less negative values are again computed) and

a marked reduction in Nusselt number magnitudes is observed. Heat transfer to the disk surface is therefore effectively controlled with ferromagnetic parameter β_1, which is advantageous in thermal regulation during spin coating operations.

Table 4: Skin friction and Nusselt number results for Mn-$ZnFe_2O_4$-nanoliquid

Pr	ε	S_T	β_1	c_f	c_g	Nu
1.0	0.1	1.0	1.0	1.5912552726	-1.4514173983	14.0425572158
3.0				1.5254516435	-1.4335569973	22.5484182770
	0.3			1.2543289497	-1.4167129996	8.2934312410
	0.5			1.1499220664	-1.4087914807	5.3129097223
		0.5		0.9897931228	-1.3849966723	7.6715795970
		0.7		1.1882657803	-1.4036757633	12.3123545067
			2.0	1.2758338290	-1.4086248031	17.2044138928
			3.0	1.0479046803	-1.3834248738	13.6750429527

Figs. 2-24 depict the GWRM solutions for axial velocity (f), radial velocity (f'), tangential velocity (g) and temperature (θ) with variations of selected thermophysical and magnetic parameters. This provides good visualization of the response of the key variables to different controlling parameters in the ferromagnetic nanofluid Von Karman swirling flow from the rotating disk, which gives insight into how the spin coating flow regime may be regulated. In all graphs both ferromagnetic Fe_3O_4 and Mn-$ZnFe_2O_4$, nanofluid cases are considered to provide a direct comparison of performance.

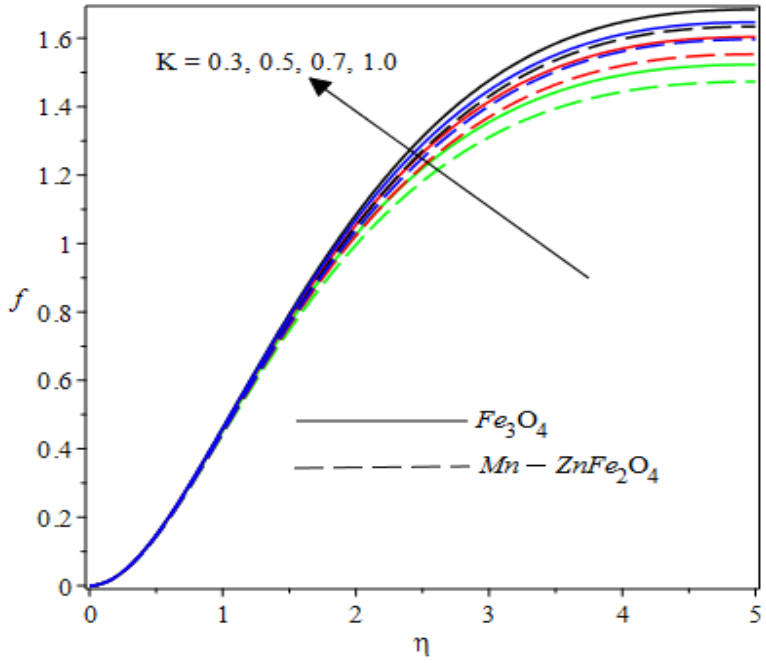

Figure 2: Axial flow rate profiles for distinct values of K

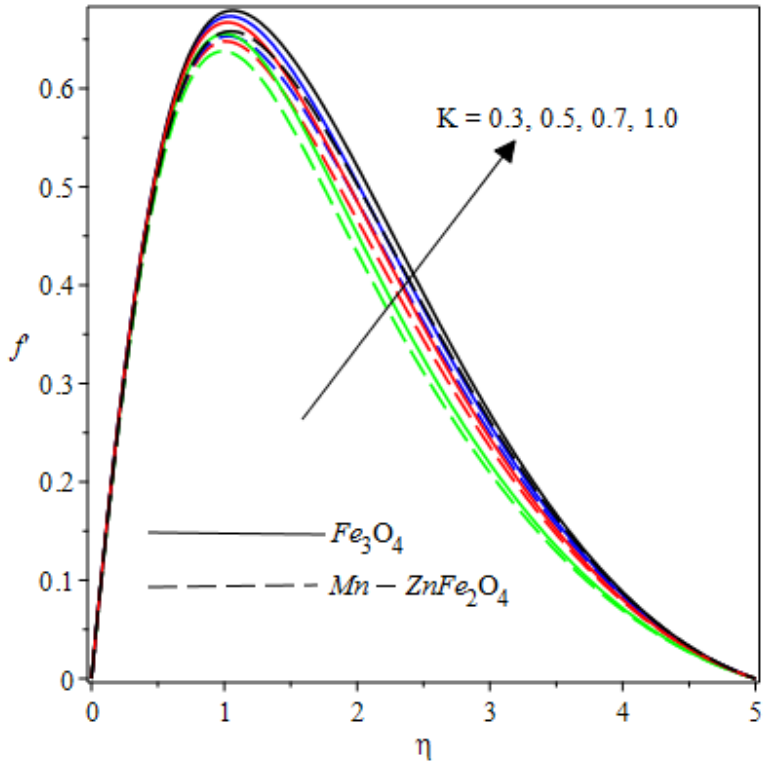

Figure 3: Radial velocity profiles for distinct values of K

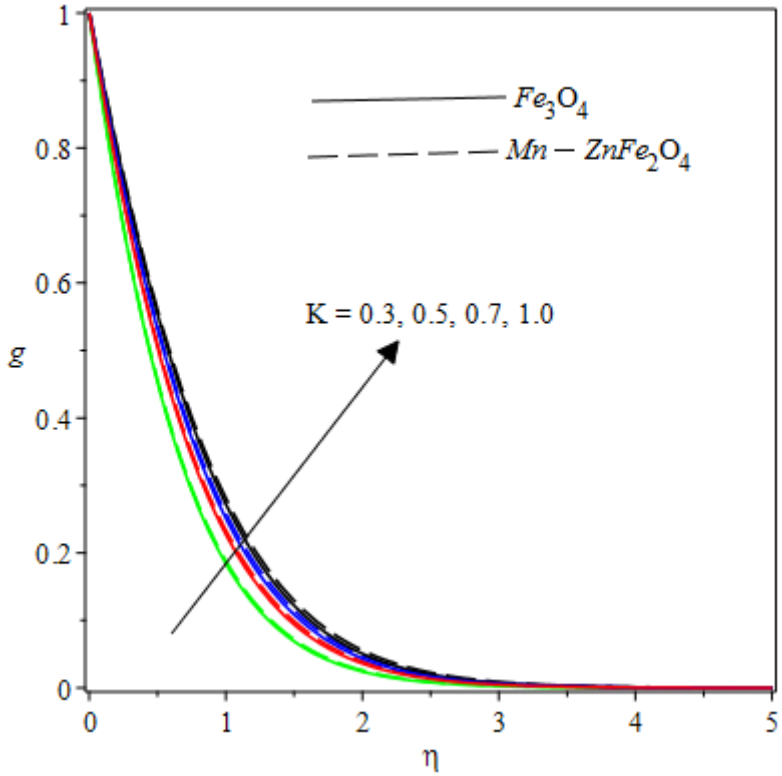

Figure 4: Tangential velocity profiles for distinct values of K

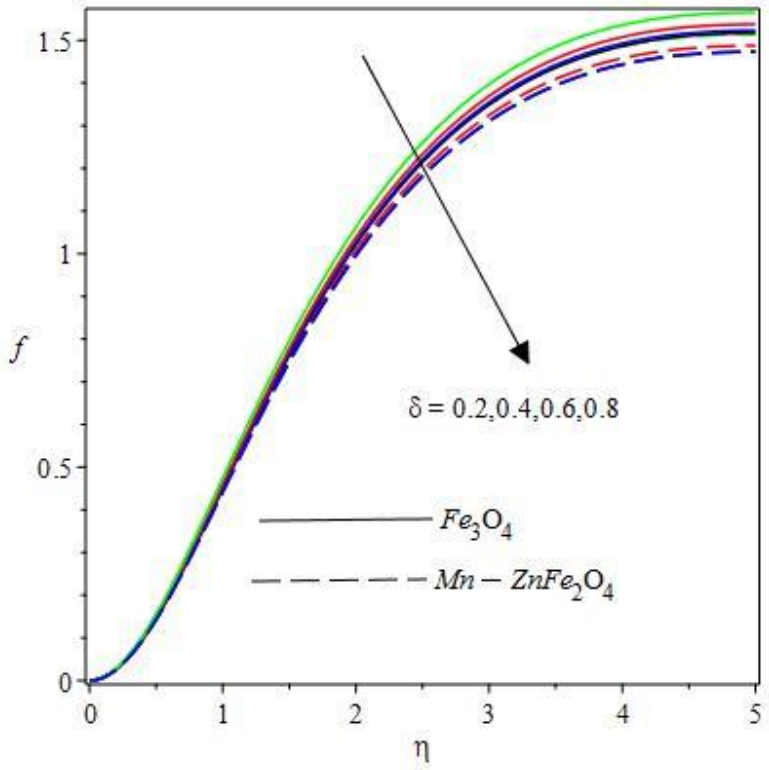

Figure 5: Axial velocity profiles for distinct values of δ

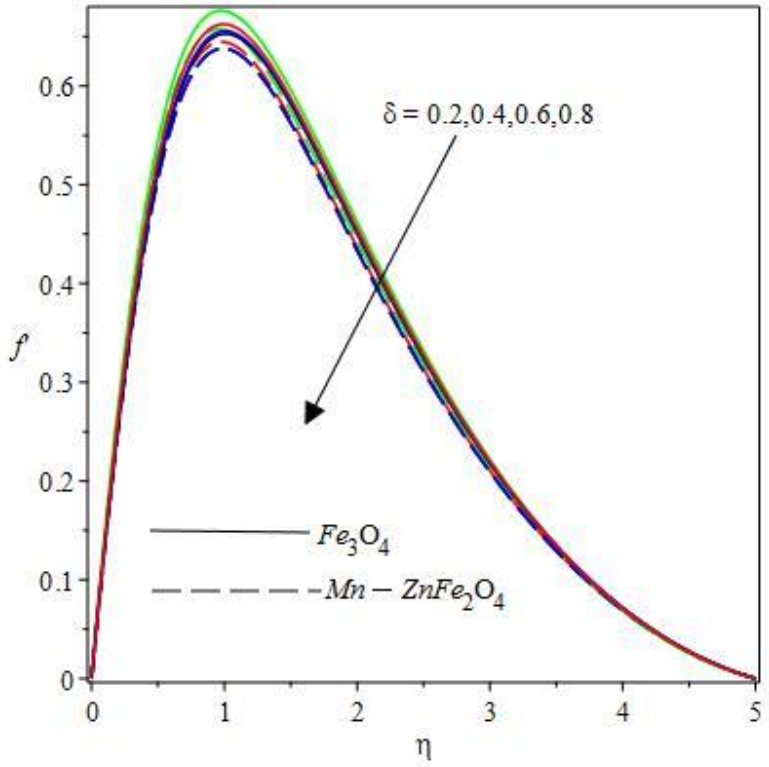

Figure 6: Radial velocity fields for distinct values of δ

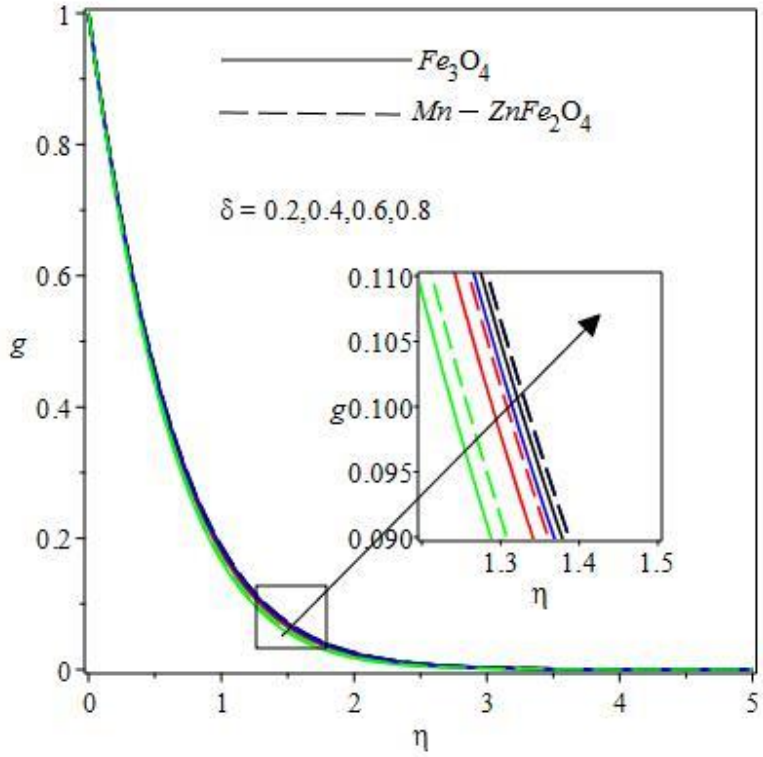

Figure 7: Tangential velocity profiles for distinct values of δ

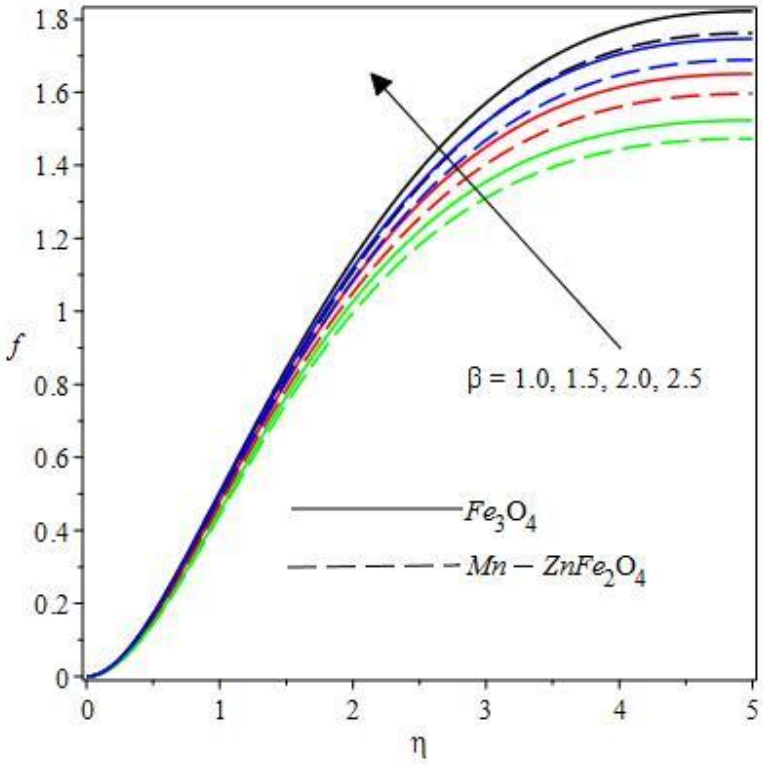

Figure 8: Axial flow rate fields for distinct values of β

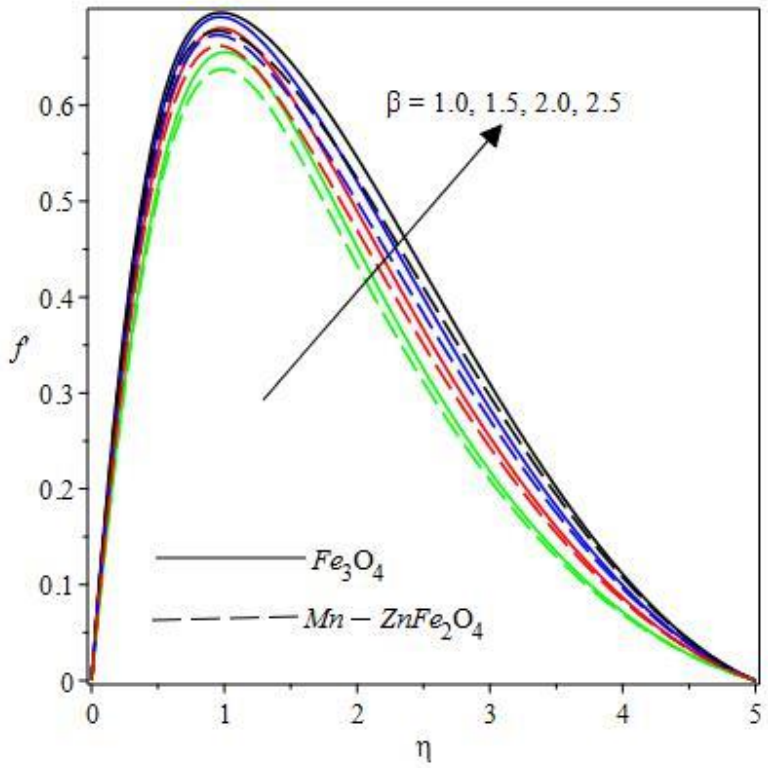

Figure 9: Radial velocity fields for distinct values of β

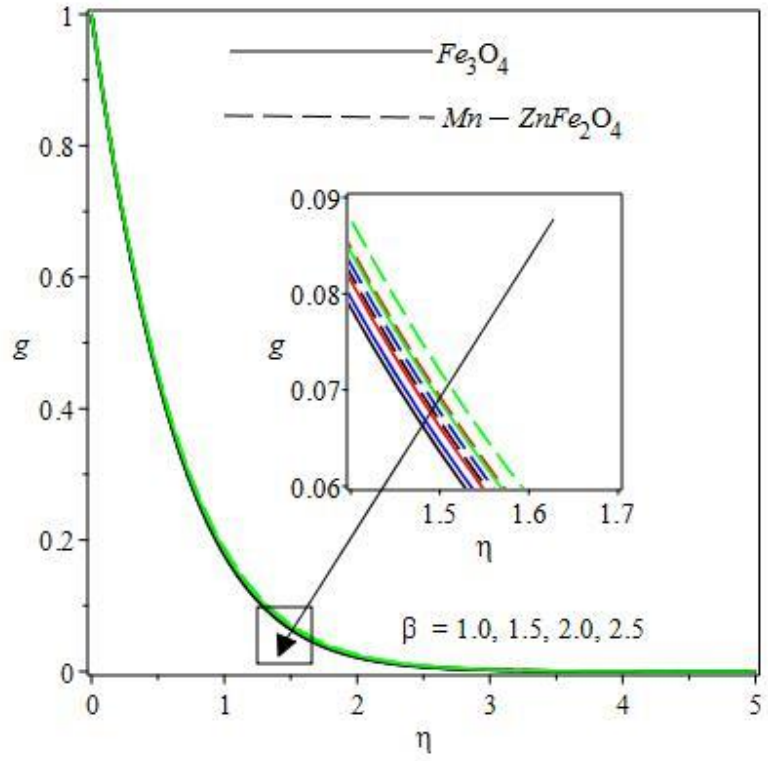

Figure 10: Tangential velocity profiles for distinct values of β

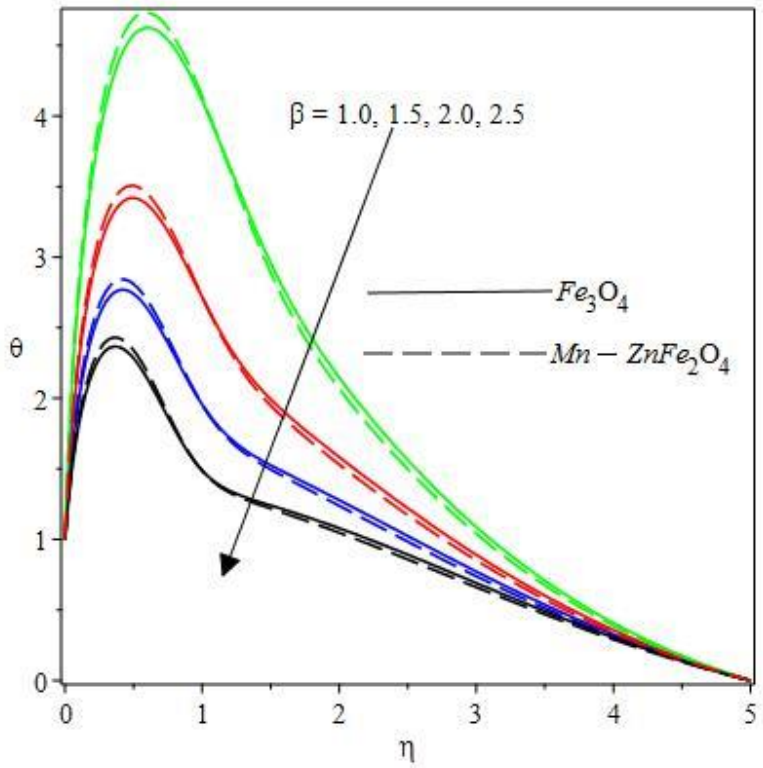

Figure 11: Temperature distributions for distinct values of β

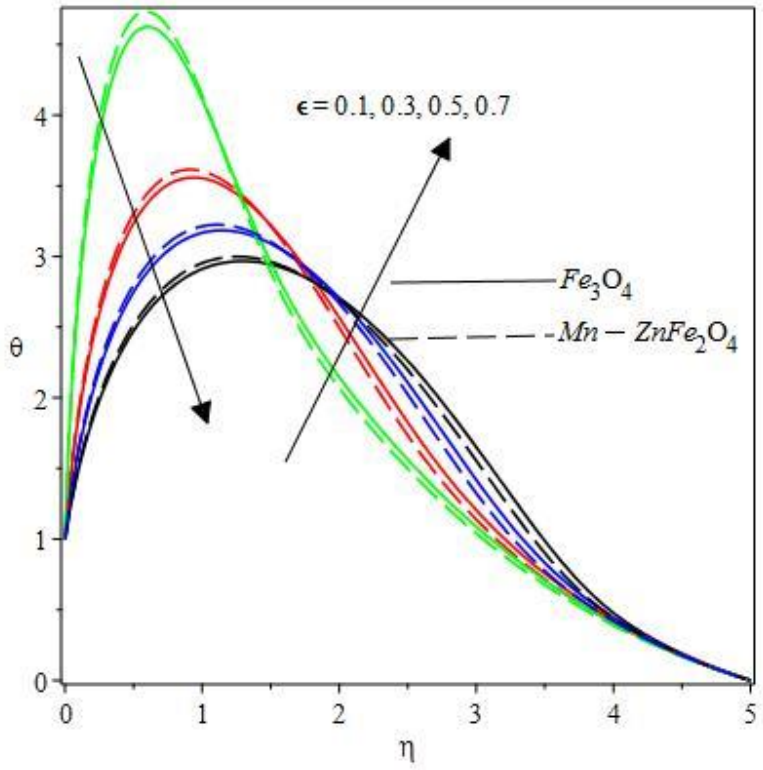

Figure 12: Temperature distributions for distinct values of ε

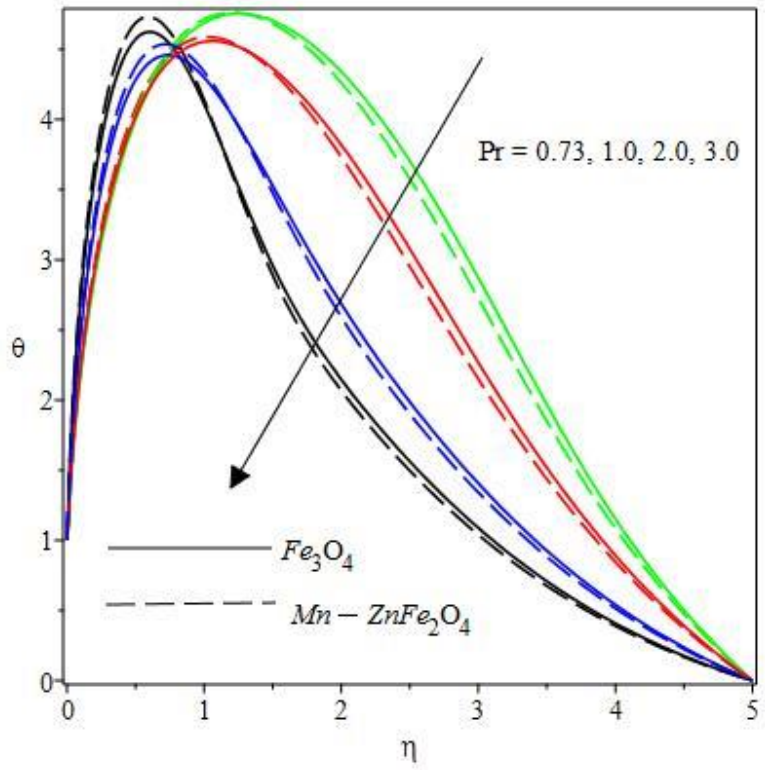

Figure 13: Temperature distributions for distinct values of Pr

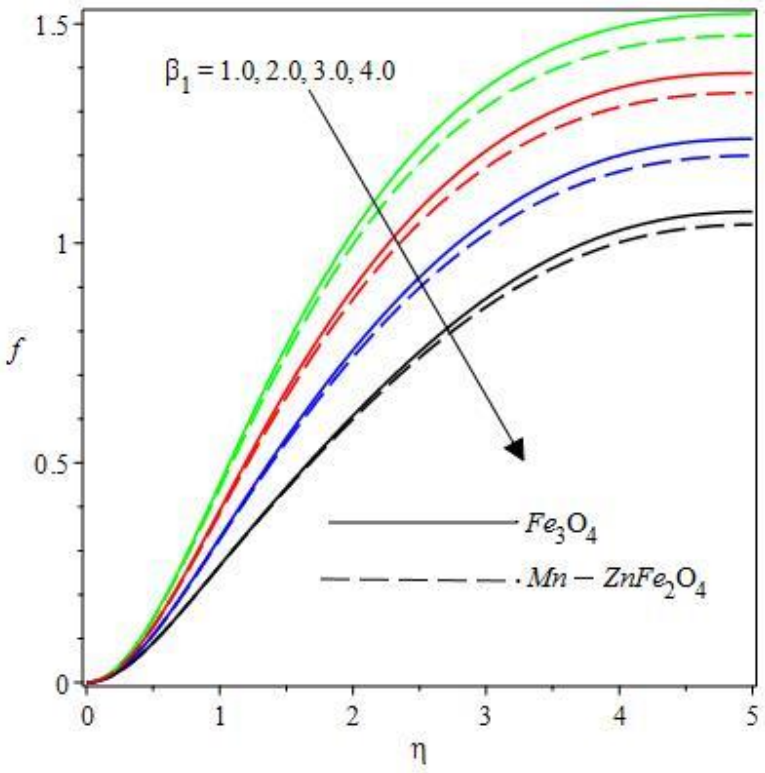

Figure 14: Axial rate profiles for distinct values of β_1

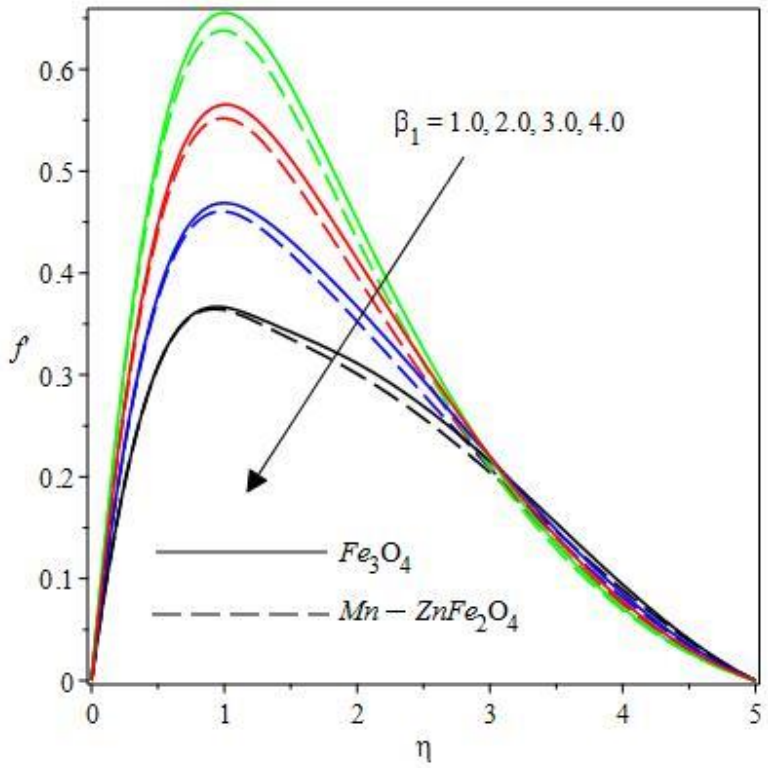

Figure 15: Radial rate profiles for distinct values of β_1

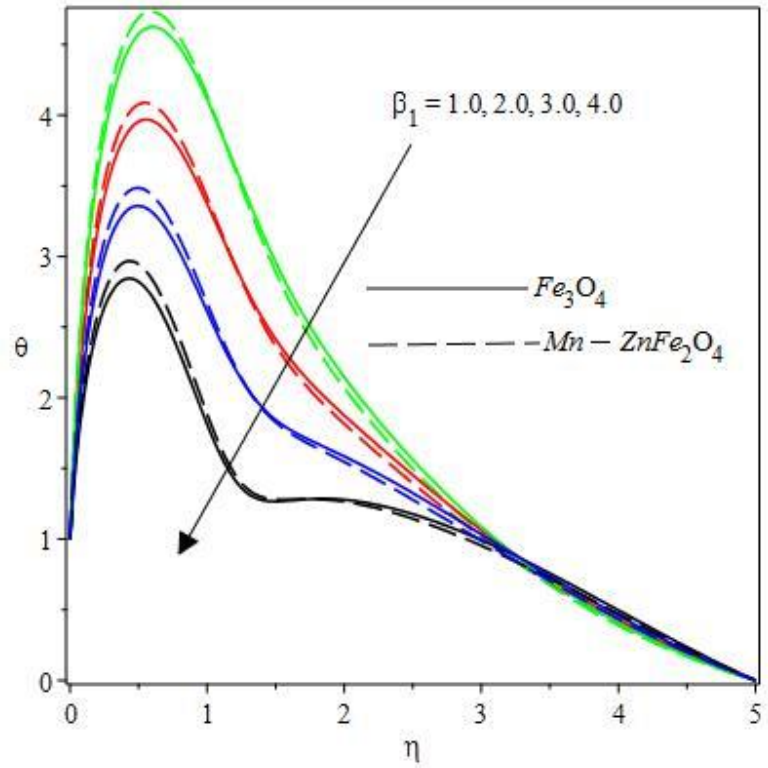

Figure 16: Temperature distribution for distinct values of β_1

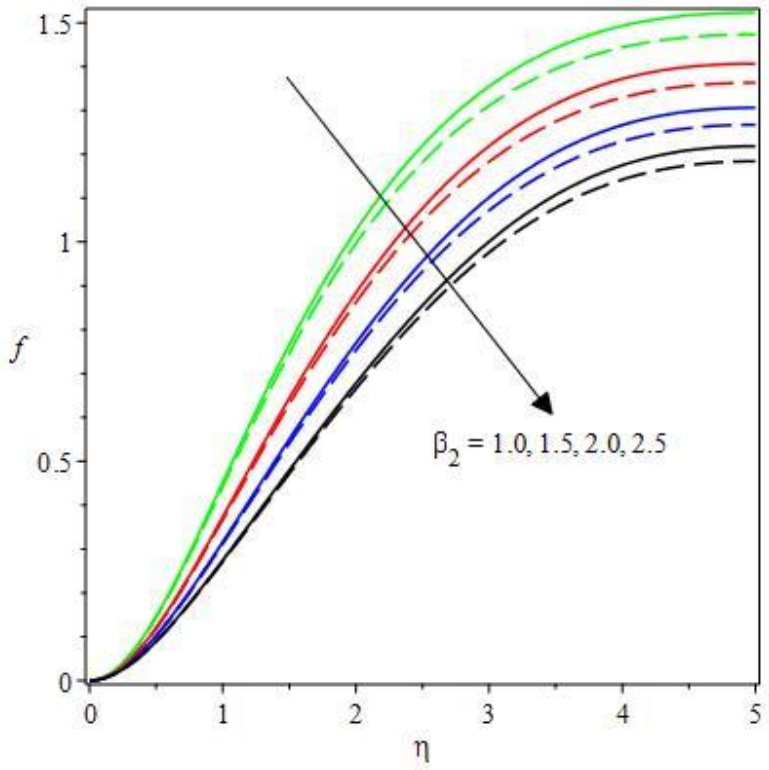

Figure 17: Axial velocity fields for distinct values of β_2

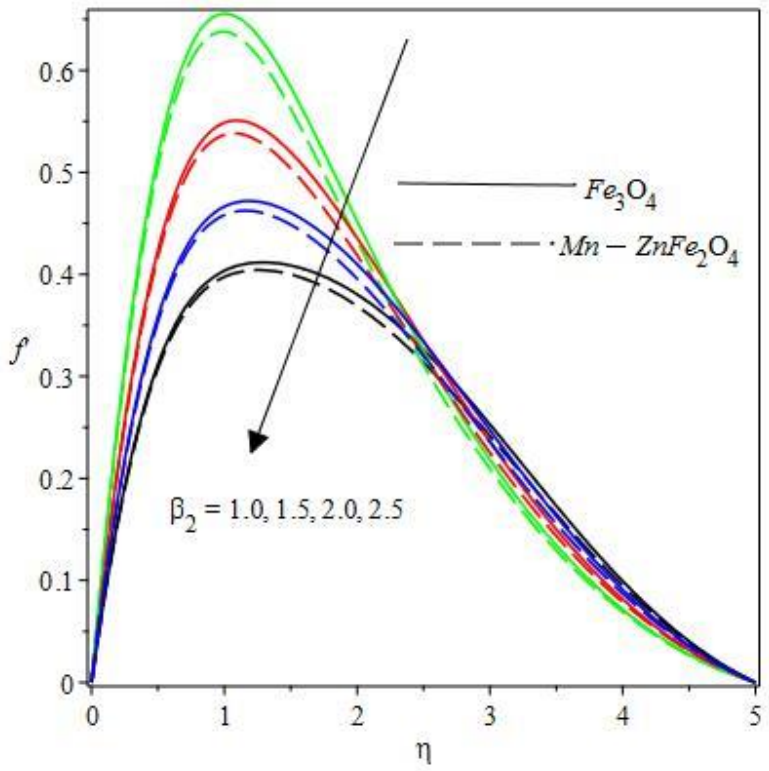

Figure 18: Radial velocity fields for distinct values of β_2

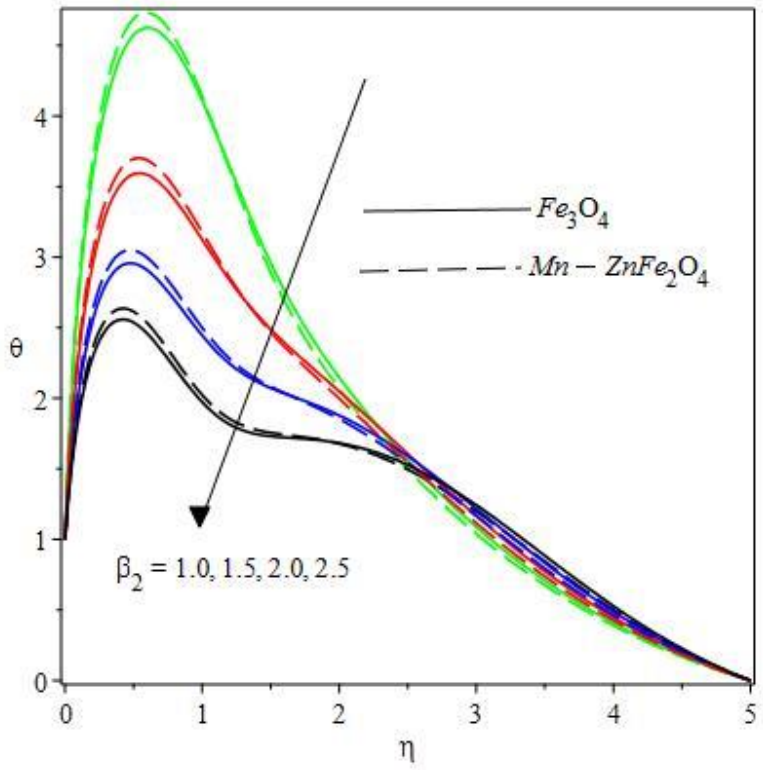

Figure 19: Temperature distributions for distinct values of β_2

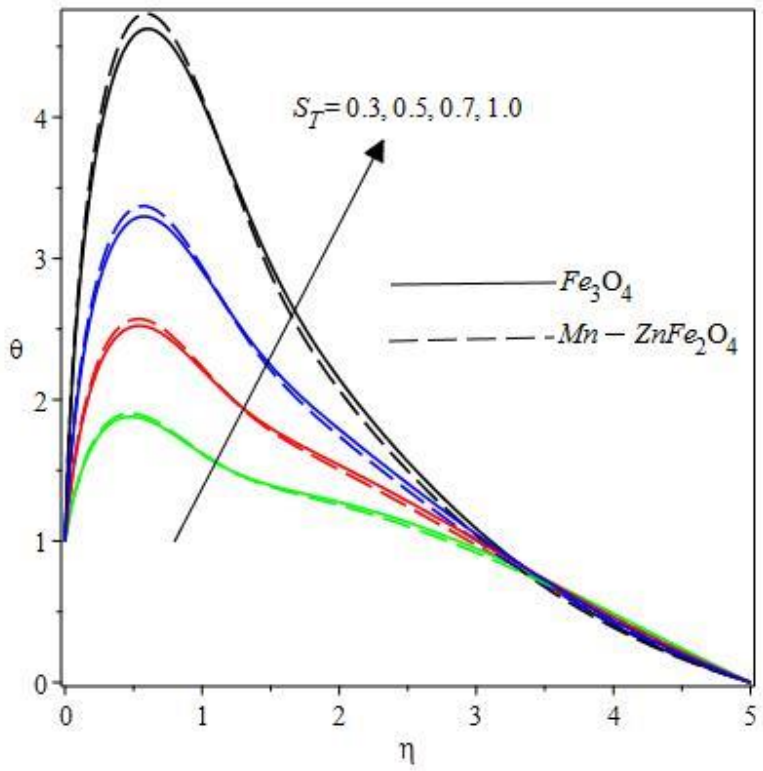

Figure 20: Temperature distributions for distinct values of S_T

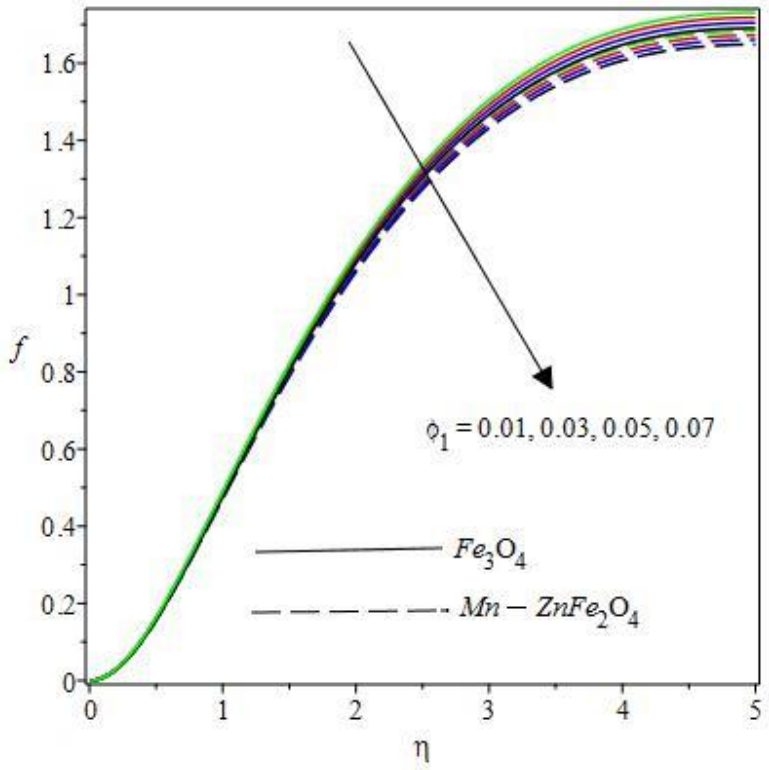

Figure 21: Axial flow rate fields for distinct values of ϕ_1

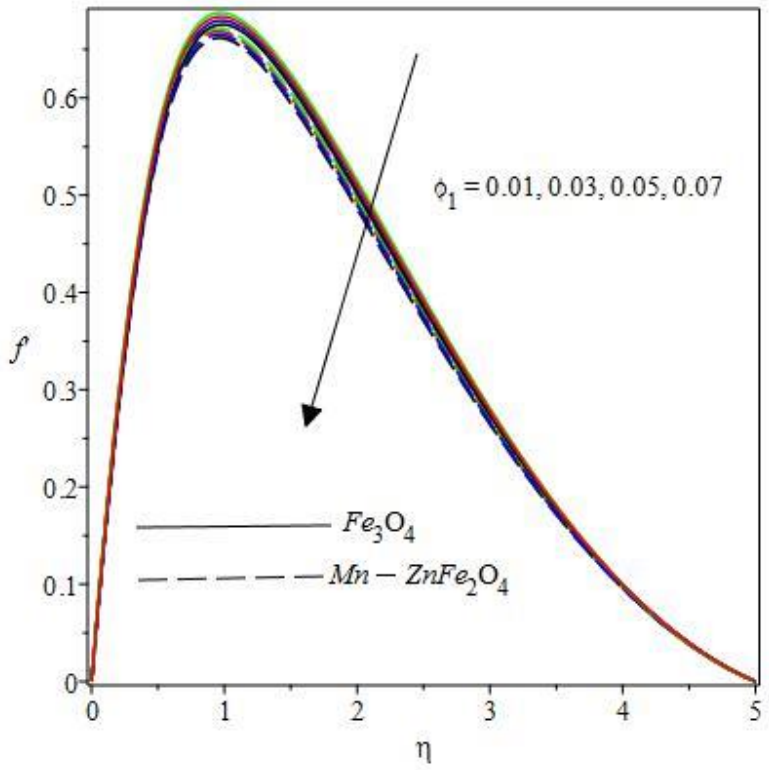

Figure 22: Radial velocity fields for distinct values of ϕ_1

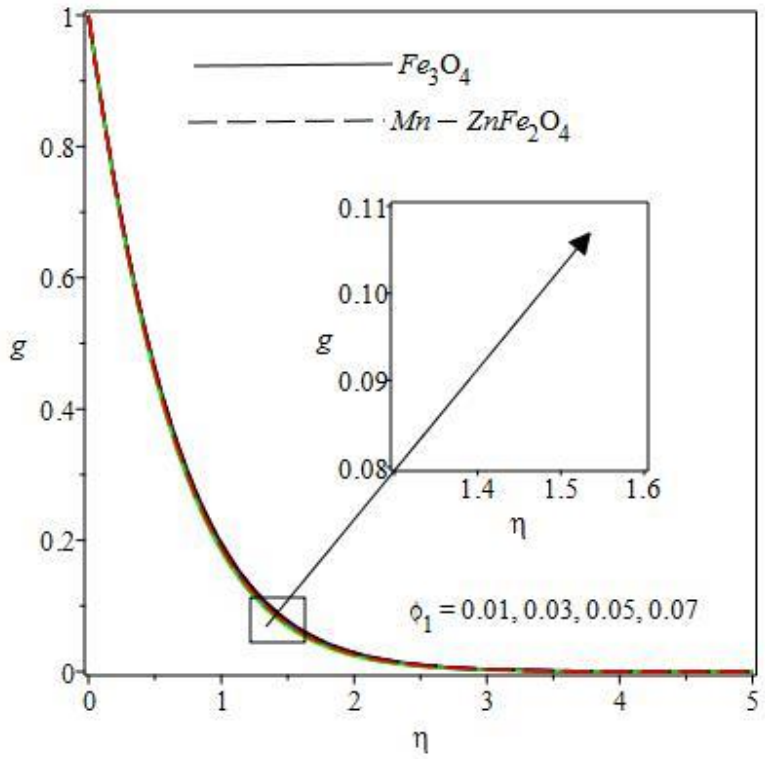

Figure 23: Tangential flow rate fields for distinct values of ϕ_1

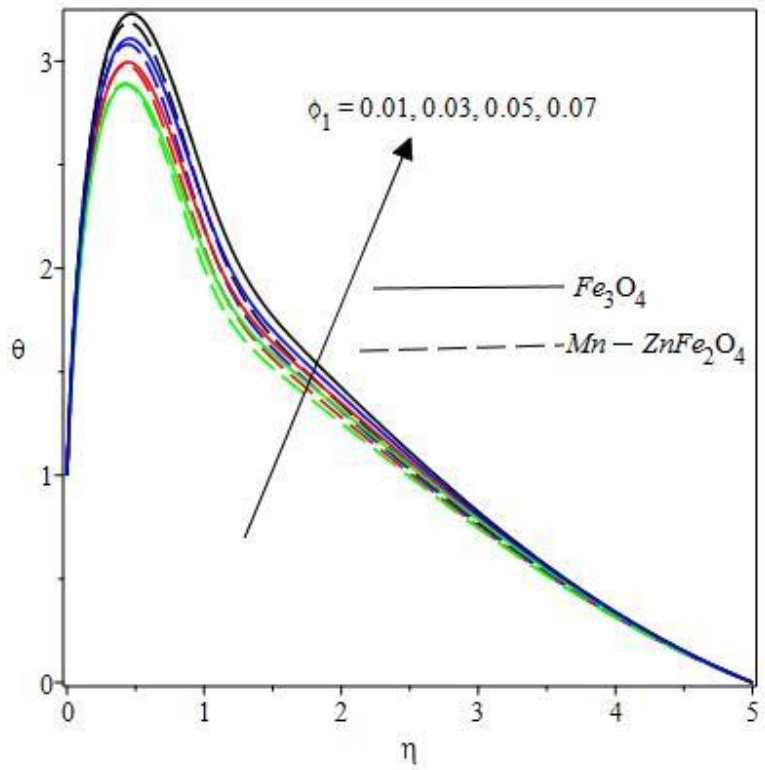

Figure 24: Temperature distributions for distinct values of nanoparticle volume fraction, ϕ_1

Figures 2 to 4 show the effect of inverse permeability parameter K on the ferromagnetic Fe_3O_4 and Mn-$ZnFe_2O_4$ nanoliquid boundary layer regime on the rotating disk. The flow velocity increases as the modified permeability parameter, $K = k_0\Omega / \nu_f$ is enhanced. The larger values of *K* imply progressive reduction in solid matrix fibers in the porous medium and this reduces the Darcian impedance component magnitudes i. e. $-\frac{K_1}{K_2 K_3}\left(\frac{1}{K} f'\right)$ in the radial momentum Eqn. (14) and $-\frac{K_1}{K_2 K_3}\left(\frac{1}{K} g\right)$ in the tangential momentum eqn. (15). Thus, the axial, radial and tangential velocities all increase with transverse axial coordinate (η). Flow acceleration is therefore successfully produced with greater porous medium permeability and deceleration is achieved with lower permeability. However, it is evident that the Fe_3O_4 -water ferromagnetic nanofluid achieves greater velocity component values than the Mn-$ZnFe_2O_4$ -water ferromagnetic nanofluid for the *axial and radial cases*, but the opposite trend is observed for the *tangential distribution*. This is probably associated both the density and viscosity of the respective ferromagnetic nanofluids and the re-distribution in the momentum between the radial and tangential components due to the pump like action of swirling flows. Clearly judicious selection of the porous medium permeability may therefore provide an excellent mechanism for regulating the spin coating flow characteristics in industrial applications. It is also likely that greater permeability associated with larger pore spaces, permits better percolation of the ferromagnetic nanoparticles and this enhanced mobility contributes to a reduction in friction at the disk surface. A smooth asymptotically profiles are consistently realized for the flow far stream establishing the description of a sufficiently high infinity boundary conditions in the GWRM numerical solutions.

Figures 5- 7 illustrate the response in axial velocity $f(\eta)$, radial velocity $f'(\eta)$ and tangential velocity $g(\eta)$ to changes in the magnetic field intensity parameter, δ. Associated with ferromagnetic effects, this parameter features in the coefficients, $K_1 = \left\{1 + \frac{3}{2}\phi_1 \frac{\delta - \tanh\delta}{\delta + \tanh\delta}\right\}$, $K_4 = \left\{\frac{k_s + 2k_f - 2\phi_1(k_f - k_s)}{k_s + 2k_f + 2\phi_1(k_f - k_s)}\right\}$ which appear in multiple terms in the transformed boundary layer model e.g. in the radial momentum Eqn. (14) in the term $\frac{K_1}{K_2 K_3}\left(2f''' - \frac{1}{K} f'\right)$, in the

tangential momentum Eqn. (15) in the term $\frac{K_1}{K_2 K_3}\left(2g'' - \frac{1}{K}g\right)$ and also in the energy Eqn. (16) in the terms, $K_4\left[\left(1+\varepsilon\theta\right)\theta'' + \varepsilon\left(\theta'\right)^2\right]$. However, it is distinct from the parameter δ_0 which denotes strength of magnetic field and is confined to the ferromagnetic parameters, $\beta = \frac{\mu_0 k_a \delta_0 \left(T_1 - T_2\right)}{\pi \rho_f \Omega^2 r^4}, \beta_1 = \frac{\mu_0 k_a \delta_0 T_c}{2\pi r^2 \left(\rho c_p\right)_f \left(T_w - T_c\right)}, \beta_2 = \frac{\mu_0 k_a \delta_0}{2\pi r^2 \left(\rho c_p\right)_f}$ as defined in Eqn. (19). As δ is elevated the coefficients K_1 *and* K_4 are clearly modified which alters the shear terms in the radial and tangential momentum equations. Both *axial and radial velocity are damped* with increasing values of δ *due to the resistive nature of the magnetization force.* However, the momentum lost in the axial and radial directions (Figs. 5, 6) is re-distributed in the tangential direction leading to a *slight increment* in tangential velocity (Fig. 7) with increasing magnetic field intensity parameter, δ, associated with the enhancement in Lorentz magnetization forces and greater nanofluid viscosity with stronger magnetic field intensity. As noted before, the Fe_3O_4 -water ferromagnetic nanofluid achieves greater axial and radial velocity component magnitudes than the Mn-$ZnFe_2O_4$ -water ferromagnetic nanofluid, but the opposite trend is observed for the tangential distribution and this is also attributable to the heating induced by the electrical current which energizes the tangential flow. Axial and radial velocities exhibit the characteristic parabolic profiles, whereas the tangential velocity shows a monotonic decrement (decay) from the disk surface to the free stream. Maximum tangential velocity is therefore always computed at the disk surface, whereas the maximum axial velocity is delayed to the free stream and the maximum radial velocity arises away from the disk surface, some distance transverse to it. These trends concur with other studies of ferromagnetic nanofluid swirling flows e.g. [28, 43]. In all profiles positive values are computed indicating that there is no flow reversal i. e. backflow is not induced anywhere in the boundary layer regime.

Figures 8-11 show the evolution in the axial flow velocity, radial velocity, tangential velocity and temperature function, with increment in ferromagnetic interaction number, β. As seen, the axial and radial flow velocity magnitudes increase with rising ferromagnetic interaction number, since this parameter energizes these flows by assisting momentum diffusion in the axial and radial direction. The expected monotonic growth in axial velocity which is characteristic of Von Karman swirling flow is clearly captured in Fig. 8. The near-wall velocity overshoot associated with radial flow is also correctly computed in Fig. 9. In both cases the respective velocity component is enhanced more distinctly with further distance from the disk

surface i.e., the profiles are more significantly enhanced deeper into the boundary layer regime away from the disk surface. Ferromagnetic nanoparticles are therefore more successfully mobilized further from the disk surface where clustering effects are minimized. However, owing to the surge in momentum in the axial and radial directions, by virtue of momentum conservation, the tangential velocity magnitudes are decreased (Fig. 10) and tangential flow retardation is produced. Temperature distribution is observed to follow a staggered parabolic topology (Fig. 11) and generally, with increasing ferromagnetic interaction number, β there is a depletion in temperatures. This is the opposite effect to that induced in conventional magnetohydrodynamic flows, as noted by Cramer and Pai [49]. Ferromagnetic nanofluids do not dissipate thermal energy in the same way as conventional electrically conducting fluids. Thermal boundary layer thickness is therefore decreased with greater ferromagnetic interaction number, β and cooling is induced in the swirling regime.

Figure 12 shows the impact of thermal conductivity parameter (ε) on the ferromagnetic nanofluid temperature distribution. `This parameter arises solely in the augmented thermal diffusion terms in the energy Eqn. (16), viz, $K_4\left[\left(1+\varepsilon\theta\right)\theta''+\varepsilon\left(\theta'\right)^2\right]$. As per the Hooman-Gurgenci formulation [41], $k(T)=k_{nf}\left\{1+\varepsilon\dfrac{T-T_\infty}{T_w-T_\infty}\right\}$ in Eqn. (7), thermal conductivity will be reduced with values of (ε) and this will have a depletive effect on temperatures near the wall (disk surface). However further from the wall, there is an *elevation in temperatures* which is sustained into the free stream. The influence of thermal conductivity parameter (ε) on temperature evolution is therefore strongly linked to the location transverse to the disk surface- at the disk surface thermal conduction is dominant whereas further into the swirling regime thermal convection becomes dominant. Furthermore, there is also a variation in the performance of the ferromagnetic nanoparticles. Closer to the disk surface the Mn-$ZnFe_2O_4$ - water ferromagnetic nanofluid achieves temperature magnitudes than the Fe_3O_4 -water ferromagnetic nanofluid, whereas further from the disk this behavior is reversed.

Figure 13 illustrates the effect of Prandtl number (Pr) on the heat transfer in the swirling boundary layer regime transverse to the rotating disk. Initially there is an *increment* in temperatures near the disk surface with greater Prandtl number, associated with clustering of ferromagnetic particles near the disk surface which energizes the flow temporarily and produces a temperature overshoot near the disk surface. However, the dominate influence of greater Prandtl number is sustained for the majority of the regime after the peak temperature, where a strong monotonic decay is observed which continues into the free stream. Thermal

boundary film viscosity is effectively decreased, and the regime is cooled. Prandtl number is inversely relative to heat conduction of the ferromagnetic nanofluid. It also expresses the momentum diffusion relation to heat diffusion. For *Prandtl number of unity*, both heat diffuse and momentum at equal rate. However, for Prandtl number lower than unity, thermal diffusion dominates which explains the higher temperatures achieved with the lowest Prandtl number (Pr = 0.73). For Prandtl number exceeding unity, there is a significant reduce in heat diffusion relative to diffusivity of the momentum. This result in a decrement in temperatures in the regime and cooling of the coating deposited. As noted earlier in close proximity to the disk surface the Mn-$ZnFe_2O_4$-water ferromagnetic nanofluid produces slightly greater temperature magnitudes than the Fe_3O_4 -water ferromagnetic nanofluid, whereas the opposite trend is computed further from the surface of the disk to the boundary film edge.

Figures 14 to 19 present the impact of ferromagnetic interaction parameters β_1 and β_2 respectively on the axial velocity, radial velocity and temperature distributions, again for both Fe_3O_4 and Mn-$ZnFe_2O_4$ nanofluids. Increment in $\beta_1 \left(= \frac{\mu_0 k_a \delta_0 T_c}{2\pi r^2 \left(\rho c_p\right)_f \left(T_w - T_c\right)} \right)$, strongly reduces both axial and radial velocity (Figs. 14, 15) and also substantially depletes the temperatures (Fig. 16). The associated ferromagnetic forces therefore damp the axial and radial flow and cool the boundary layer, decreasing thermal boundary layer thickness. Similarly, there strong damping in the axial and radial flow generated with increment in $\beta_2 \left(= \frac{\mu_0 k_a \delta_0}{2\pi r^2 \left(\rho c_p\right)_f} \right)$ as observed in Figs. 17, 18. Temperatures are also strongly suppressed with greater β_2 *values* (Fig. 19) implying that once again thermal boundary layer thickness is depleted. There is a strong influence of both ferromagnetic parameters experienced in the energy Eqn. (16) via the terms, $-\mathrm{Pr}\,\beta_1 f'$, $--\mathrm{Pr}\,\beta_2 f'\theta$ which inhibit momentum diffusion and also counteract thermal diffusion. This manifests in the trends reported in Figs. 14-19 and concurs with previous studies including [29] and [31].

Figure 20 depicts the variation in temperature distribution with transverse (axial) coordinate for an increase in the heat generation temperature-dependent (source) term S_T . An enhance in the heat generation generates significant thermal energy in the boundary layer regime which enhances thermal diffusion and boosts temperatures. There is a marked elevation also in thermal boundary layer thickness. Heat source effectively augments the thermal conductivity boos achieved with ferromagnetic nanoparticles. Further from the disk surface, Fe_3O_4

nanoparticles achieve temperatures in excess of those computed for Mn-$ZnFe_2O_4$ nanoparticles. Mn-$ZnFe_2O_4$ -water ferromagnetic nanofluid is therefore shown to achieve *lower thermal conductivity enhancement* relative to Fe_3O_4-water ferromagnetic nanofluid. The opposite trend is observed closer to the disk surface.

Finally, **Figs. 21-24** illustrate the influence of nanoparticle volume concentration (ϕ_1) on flow velocity components and temperature field. Volume fraction effects are simulated via all five coefficients, $K_1 = \left\{1+\frac{3}{2}\phi_1\frac{\delta-\tanh\delta}{\delta+\tanh\delta}\right\}$, $K_2 = \left\{1-\phi_1\right\}^{2.5}$, $K_3 = \left\{1-\phi_1+\phi_1\frac{\rho_s}{\rho_f}\right\}$, $K_4 = \left\{\frac{k_s+2k_f-2\phi_1(k_f-k_s)}{k_s+2k_f+2\phi_1(k_f-k_s)}\right\}$, $K_5 = \left\{1-\phi_1+\phi_1\frac{(\rho c_p)_s}{(\rho c_p)_f}\right\}$, as defined in Eqn. (18), as per the Tiwari-Das nanoscale formulation.

Axial and radial velocities (Figs. 21, 22) are depleted with greater nanoparticle volume fraction, whereas the tangential (azimuthal) velocity (Fig. 23) is weakly enhanced. The damping in the axial and flow radial is associated with increasing magnetic viscosity which impedes these flows. However, tangential acceleration is attained via a momentum re-distribution in the swirling regime. Temperatures are clearly strongly elevated with nanoparticle volume concentration (ϕ_1) from 0.01 (1% doping) through 0.03, 0.05 to a maximum of 0.07 (7% doping). The key characteristic of nanofluids i. e. thermal enhancement is therefore confirmed in Fig. 24, for low doping percentages of ferromagnetic nanoparticles. The heat conduction and liquid viscosity are favorably modified with nanoparticle presence, which via ballistic collisions effectively encourages a growth in heat boundary film viscidness in the swirling coating region.

5. Conclusions

In the analysis, a mathematical formulation is developed for steady swirling Von Karman flow and thermal transport in nanofluids water-based having ferromagnetic nanoparticles from a rotating disk in Darcian permeable media. The Odenbach formulation is deployed for magnetic field fluid viscosity dependent and the Hooman- Gurgenci model is used for variable thermal conductivity. The governing conservation model for the mass, momentum and heat are converted into nonlinear coupled ordinary derivative momentum and energy equations via appropriate similarity transformations with appropriate boundary conditions. A nanoscale Tiwari-Das model is deployed for the fractional volume nanoparticle effects. The resulting

ordinary differential boundary value problem is analytically solved with a Galerkin weighted residual method (GWRM) along with Simpson's one-third rule. Verification of the GWRM solutions is achieved with numerical quadrature (MAPLE) and very good correlation is demonstrated. The main results for the current study can be abridged as follows:

- Ferromagnetic Fe_3O_4 nanofluid is observed to achieve superior thermal conductivity enhancement relative to ferromagnetic Mn-$ZnFe_2O_4$ nanofluid.
- Increasing magnetic field intensity parameter (δ) produces a significant elevation in fluid viscosity which damps both the axial and radial flow; however weak tangential flow acceleration is produced.
- Increasing permeability parameter (K) enhances axial, radial and tangential velocity magnitudes and, in all cases, the Fe_3O_4-water ferromagnetic nanofluid achieves greater values than the Mn-$ZnFe_2O_4$-water ferromagnetic nanofluid, in particular at intermediate distances from the disk surface (axial coordinate).
- With greater ferromagnetic interaction number (β) axial velocity is enhanced strongly, and radial velocity is also boosted. However tangential velocity is slightly reduced, and temperature is strongly suppressed for both ferromagnetic nanofluids.
- With increasing Prandtl number (Pr), temperatures are strongly decreased whereas they are elevated with increasing heat source (generation) parameter (S_T).
- Heat transfer to the disk surface is very effectively controlled with ferromagnetic parameter (β_1) which is advantageous in thermal regulation during spin coating operations.
- Axial and radial velocities are significantly damped with greater nanoparticle volume fraction, whereas the tangential (azimuthal) velocity (Fig. 23) is weakly enhanced. Temperatures are substantially elevated with nanoparticle volume concentration (ϕ_1)
- A significant deceleration in axial and radial flow is produced with increment in ferromagnetic parameter β_2 as observed and temperatures are also strongly depleted as is thermal boundary layer thickness is depleted.
- With greater thermal conductivity parameter (ε) there is a significant reduction in radial skin friction, c_f and Nusselt number, but a weak increase in tangential skin friction, c_g.

The present study has neglected *unsteady* flow and *viscoelastic non-Newtonian* characteristics which may also be encountered in ferromagnetic nanofluids. These will be explored in the future.

Data availability statement

No new data were created or analyzed in this study

References

[1] A. Bozhko, S. Suslov, *Convection in Ferro-Nanofluids: Experiments and Theory, Physical Mechanisms, Flow Patterns, and Heat Transfer*, Springer, Germany, 2018.

[2] J. Giri, P. Pradhan, V. Somani, H. Chelawat, S. Chhatre, R. Banerjee, D. Bahadur, Synthesis and characterizations of water-based ferrofluids of substituted ferrites [Fe1-xBxFe2O4, B=Mn, Co (x=0-1)] for biomedical applications, J. Magn. Magn. Mater. 320 (2008) 724–730. https://doi.org/10.1016/j.jmmm.2007.08.010.

[3] Y.O. Tu, Mathematical modelling and computer simulation spin coating of ferrofluid, IEEE Transc. Magnetics. 24 (1988) 3129 – 3131.

[4] M. Zahn, Magnetic fluid and nanoparticle applications to nanotechnology, J. Nanopart. Res. 3 (2001) 73-78.

[5] I. Torres-Díaz, C. Rinaldi, Recent progress in ferrofluids research: novel applications of magnetically controllable and tunable fluids, Soft Matter. 10 (2014) 8584–8602.

[6] D. Tian, N. Zhang, X. Zheng, G. Hou, Y. Tian, Y. Du, L. Jiang, S.X. Dou, Fast responsive and controllable liquid transport on a magnetic fluid/nanoarray composite interface, ACS Nano 10(6) (2016) 6220–6226.

[7] H. Kuroki, I. Tokarev, S. Minko, Responsive surfaces for life science applications, Annu. Rev. Mater. Res. 42 (2012) 343–372.

[8] M. Kole, S. Khandekar, Engineering applications of ferrofluids: A review, J. Magn. Magn. Mater. 537 (2021) 168222. https://doi.org/10.1016/j.jmmm.202.168222

[9] M. Arana, P.G. Bercoff, S.E. Jacobo, Thermomagnetic characterization of organic-based ferrofluids prepared with Ni ferrite nanoparticles, Mat. Sci. Eng. B. 215 (2017) 1-8.

[10] R.E. Rosensweig, *Ferrohydrodynamics*, Cambridge University Press, Cambridge, New York, 1985.

[11] A. Chaves, M. Zahn, C. Rinaldi, Spin-up flow of Ferro fluids: Asymptotic theory and experimental measurements, Phys. Fluids. 20 (2008) Article ID: 053102. https://doi.org/10.1063/1.2907221

[12] S. Odenbach, L.M. Pop, A.Y. Zubarev, Rheological properties of magnetic fluids and their microstructural background, GAMM-Mitteilungen. 30(10) (2007) 195–204. https://doi.org/10.1002/gamm.200790008

[13] M. Sheikholeslami, S.A. Shehzad, Numerical analysis of Fe_3O_4–H_2O nanofluid flow in permeable media under the effect of external magnetic source, Int. J. Heat Mass Transf. 118 (2018) 182–192. https://doi.org/10.1016/j.ijheatmasstransfer.2017.10.113

[14] B. Mahanthesh, B.J. Gireesha, S.A. Shehzad, A. Rauf, P.B.S. Kumar, Nonlinear radiated MHD flow of nanoliquids due to a rotating disk with irregular heat source and heat flux condition, Phys. B Condensed Matter. 537 (2018) 98–104. https://doi.org/10.1016/j.physb.2018.02.009

[15] A. Gavili, F. Zabihi, T.D. Isfahani, J. Sabbaghzadeh, The thermal conductivity of water base ferrofluids under magnetic field, Exp. Therm. Fluid Sci. 41 (2012) 94–98. https://doi.org/10.1016/j.expthermflusci.2012.03.016

[16] N. Gan Jia Gui, C. Stanley, N.T. Nguyen, G. Rosengarten, Ferro fluids for heat transfer enhancement under an external magnetic field, Int. J. Heat and Mass Transf. 123 (2018) 110-121. https://doi.org/10.1016/j.ijheatmasstransfer.2018.02.100.

[17] Z. Josip, M.R. Marijana, Thermal and rheological properties of water-based ferrofluids and their applicability as quenching media, Phys. Procedia. 7 (2015) 1458-1467. https://doi.org/10.1016/j.phpro.2015.12.166

[18] Q. Li, J. Zhao, L. Jin, D. Li, Experimental study on thermal conductivity and magnetization behaviors of kerosene-based ferrofluid loaded with multiwalled carbon nanotubes, ACS Omega. 5 (2020) 13052-13063. https://doi.org/10.1021/acsomega.Dc00964

[19] A. Bhandari, Water-based Ferro fluid flow and heat transfer over a stretchable rotating disk under the influence of an alternating magnetic field, Proc. IMechE Part C: J. Mech. Eng. Sci. 235(12) (2020) 2201-2214. https://doi.org/10.1177/094406220952515

[20] A. Mehmood, Asif Ali, H. S. Takhar, **O. Anwar Bég**, M.N. Islam, L.S. Wilson, Unsteady Von Kármán swirling flow: analytical study using the Homotopy Method, Int. J. Appl. Math. Mech. 6(2) (2010) 67 – 84.

[21] S.R. Mishra, MD. Shamshuddin, **O. Anwar Bég**, Ali Kadir, Numerical study of heat transfer and viscous flow in a dual rotating extendable disk system with a non-Fourier heat flux model, Heat Transf. 48(1) (2019) 435-459.

[22] **O. Anwar Bég**, J. Zueco, L.M. López-Ochoa, Network numerical analysis of optically thick hydromagnetic slip flow from a porous spinning disk with radiation flux, variable

thermophysical properties and surface injection effects, Chem. Eng. Commun. 198 (3) (2011) 360-384.

[23] T. Hayat, S. Qayyum, M. Imtiaz, A. Alsaedi, Flow between two stretchable rotating disks with Cattaneo-Christov heat flux model, Results in Phys. 7 (2017) 126-133.

[24] M. Turkyilmazoglu, Nanofluid flow and heat transfer due to a rotating disk, Comput. Fluids. 94 (2014) 139–146. https://doi.org/10.1016/j.compfluid.2014.02.009

[25] O. Anwar Bég, N. Kabir, M.J. Uddin, A.I.M. Ismail, Y. Alginahi, Numerical investigation of Von Karman swirling bioconvective nanofluid transport from a rotating disk in a porous medium with Stefan blowing and anisotropic slip effects, Proc. IMechE- Part C- J. Mech. Eng. Sci. (2020). https://doi.org/10.1177/0954406220973061

[26] J.C. Umavathi, S.L. Patil, B. Mahanthesh, **O. Anwar Bég**, Unsteady squeezing flow of magnetized nano-lubricant between parallel disks with Robin boundary condition, Proc. IMechE J. Nanomat. Nanoeng. Nanosyst. (2020). https://doi.org/10.1177/23977914211036562

[27] P. Ram, V. Kumar, Ferrofluid flow with magnetic field dependent viscosity due to rotating disk in porous medium, Int. J. Appl. Mech. 4(4) (2012) 1250041. https://doi.org/10.1142/S175882511250041X

[28] A. Bhandari, Study of ferrofluid flow in a rotating system through mathematical modelling, Math. Computers Simul. 178 (2020) 290-306. https://doi.org/10.1016/j.matcom.2020.06.018

[29] I. Mustafa, J. Tariq, A. Ghaffari, Heat transfer in MHD stagnation point flow of a ferrofluid over a stretchable rotating disk, J. Mol. Liq. 219 (2016) 526-532. https://doi.org/10.1016/j.molliq.2016.03.046

[30] R. Ellahi, M.H. Tariq, M. Hassan, K. Vafai, On the boundary layer nano-ferroliquid flow under the influence of low oscillating stretchable rotating disk, J. Mol. Liq. 229 (2017) 339-345. https://doi.org/10.1016j.molliq.2016.12.073

[31] M. Mustafa, J. A. Khan, T. Hayat, A. Alsaedi, Numerical solutions for radiative heat transfer in ferrofluid flow due to a rotating disk: Tiwari and Das model, Int. J. Nonlinear Sci. Numer. Simul. 19(1) (2018) 1-10. https://doi.org/ 10.1515/ijnsns-2015-01916.

[32] V. Loganayagi, P.K. Kameswaran, Magneto hydrodynamic and heat transfer impacts on ferrofluid over a rotating disk: An application to hard disk drives, ASME J. Therm. Sci. Eng. Appl. 13(1) (2021) 011001. https://doi.org/10.1115/1.4047007.

[33] J. Ahmed, M. Khan, L. Ahmad, Swirling flow of Maxwell nanofluid between two coaxially rotating disks with variable thermal conductivity, J. Braz. Soc. Mech. Sci. Eng. 41(2019) 97. https://doi.org/10.1007/s40430-019-1589-y

[34] G.C. Hazarika, J. Borah, Effects of variable viscosity and thermal conductivity on MHD flow over a radially stretching disk, J. Computer Math. Sci. 9(9) (2018) 1282-1291. https://dx.doi.org/10.29055/jcms/869.

[35] J. Konch, G.C. Hazarika, Effects of variable viscosity and variable thermal conductivity on hydromagnetic dusty fluid flow due to a rotating disk, Front. Heat Mass Transf. 8 (2017) 39. https://doi.org/10.5098/hmt.8.39.

[36] S. Shaw, A.S. Dogonchi, M.K. Nayak, O.D. Makinde, Impact of entropy generation and nonlinear thermal radiation on Darcy-Forchheimer flow of $MnFe_2O_4$-Casson/water nanofluid due to a rotating disk: Application to brain dynamics, Arabian J. Sci. Eng. 45(7) (2020) 5471-5490.

[37] S. Das, S. Chakraborty, R.N. Jana, O.D. Makinde, Entropy analysis of nanofluid flow over a convectively heated radially stretching disk embedded in a porous medium. J. Nanofluids. 5(1) (2016) 48-58.

[38] S. Shateyi, O.D. Makinde, Hydromagnetic stagnation-point flow towards a radially stretching convectively heated disk, Math. Prob. Eng. 2013 (2013) 616947. https://doi.org/10.1155/2013/616947

[39] M. Renzi, P. Mignini, G. Giuli, R. Marassi, F. Nobili, Rotating disk electrode study of $Pt/Cs_3HPMo_{11}VO_{40}$ composite catalysts for performing and durable PEM fuel cells, Int. J. Hydrogen Energy. 41(26) (2021) 11163-11173.

[40] H. Ilyas, I. Ahmad, M.A.Z. Raja, M.B. Tahir, M. Shoaib, Neuro-intelligent mappings of hybrid hydro-nanofluid Al_2O_3–Cu–H_2O model in porous medium over rotating disk with viscous dissolution and Joule heating, Int. J. Hydrogen Energy. 46 (55) (2021) 28298-28326.

[41] H Kakisawa, N.T.B. Diem, T. Sumitomo, Y. Kagawa, Room temperature fabrication of SiO_2/polyacrylic ester multilayer composites by spin-coating, Mat. Sci. Eng. B. 173(1-3) (2010) 94-98.

[42] O.D. Makinde, F. Mabood, W.A. Khan, M.S. Tshehla, MHD flow of a variable viscosity nanofluid over a radially stretching convective surface with radiative heat, J. Mol. Liq. 219 (2016) 624-630.

[43] M. Abdel-Wahed, M. Akl, Effect of Hall current on MHD flow of a nanofluid with variable properties due to a rotating disk with viscous dissipation and nonlinear thermal radiation, AIP Adv. 6 (2016) 095308. https://doi.org/10.1063/1.4962961

[44] S. Odenbach, Magneto viscous effects in ferrofluids, Appl. Rheol. 10 (2000) 178–184. https://doi.org/10.1515/arh-2000-0011

[45] K. Hooman, H. Gurgenci, Effects of temperature-dependent viscosity variation on entropy generation, heat and fluid flow through a porous-saturated duct of rectangular cross-section, Appl. Math. Mech. 28 (2007) 69–78. https://doi.org/10.1007/s10483-007-0108-z

[46] R.A. Oderinu, Y.A.S. Aregbesola, Using Laguerre's quadrature in the weighted residual method for problems with semi-infinite domain, Int. J. Pure and Appl. Math. 75(3) (2012) 123-129.

[47] S.O. Salawu, A.B. Disu, M.S. Dada, On criticality for a generalized Couette flow of a branch-chain thermal reactive third-grade fluid with Reynold's viscosity model. The Sci. World J. 20 (2020) 7915954. https://doi.org/10.1155/2020/7915954.

[48] S.O. Salawu, S.S. Okoya, On criticality for a branched-chain thermal reactive-diffusion in a cylinder. Combust. Sci. Tech. 192 (2020) 1-16.
https://doi.org/10.1080/00102202.2020.1837120

[49] K.C. Cramer and S.I. Pai, *Magnetofluid Dynamics for Engineers and Applied Physicists*, McGraw-Hill, New York, USA, 1973.